Title

SMYD2-Mediated Histone Methylation Contributes to HIV-1 Latency

Journal

Cell Host & Microbe, 21(5)

ISSN

1931-3128

Authors

Boehm, Daniela

Jeng, Mark

Camus, Gregory

et al.

Publication Date

2017-05-01

DOI

10.1016/j.chom.2017.04.011

Peer reviewed

Regulation of HIV-1 Latency via SMYD2-Mediated Histone Methylation

Daniela Boehm[1,2], Mark Jeng[1,2], Gregory Camus[1,2], Andrea Gramatica[1,2,3], Roland Schwarzer[1,2,3], Jeffrey R. Johnson[1,4] , Philip A. Hull[1,2], Mauricio Montano[1,2,3], Naoki Sakane[1,5], Sara Pagans[1,2], Robert Godin[6], Steven G. Deeks[2], Nevan J. Krogan[1,4], Warner C. Greene[1,2,3], and Melanie Ott[1,2]*

[1]Gladstone Institute for Virology and Immunology, University of California San Francisco, San Francisco, California 94158, USA; [2]Department of Medicine, University of California San Francisco, San Francisco, CA 94143, USA; [3]Department of Microbiology and Immunology, University of California, San Francisco, San Francisco, CA 94143, USA; [4]Department of Cellular and Molecular Pharmacology, The California Institute for Quantitative Biomedical Research, University of California, San Francisco, San Francisco, CA 94158, USA; [5]Pharmaceutical Frontier Research Laboratory, JT, 1-13-2 Fukuura, Kanazawa-ku, Yokohama, Kanagawa 236-0004, Japan; [6]AstraZeneca, Boston, MA, USA

*To whom correspondence should be addressed:
Melanie Ott, MD, PhD
Gladstone Institute of Virology and Immunology, University of California San Francisco
1650 Owens Street San Francisco, CA 94158.
Tel: 415-734-4807;
E-mail: mott@gladstone.ucsf.edu

Keywords: HIV, Latency, SMYD2, H4K20me1, L3MBTL1

Summary

Transcriptional latency of the human immunodeficiency virus (HIV-1) is a last barrier to viral eradication, but the underlying mechanisms are incompletely understood. We performed an RNAi-based screen of human lysine methyltransferases and identified the SET and MYND domain-containing protein 2 (SMYD2) as a new enzyme that regulates HIV-1 latency. Knockdown of SMYD2 or its pharmacological inhibition reactivated latent HIV-1 in T-cell lines and in primary $CD4^+$ T cells. SMYD2 associated with latent HIV-1 promoter chromatin, which was enriched in monomethylated lysine 20 at histone H4 (H4K20me1), a mark lost in cells lacking SMYD2. H4K20me1 is recognized by lethal 3 malignant brain tumor 1 (L3MBTL1), a reader protein with chromatin-compacting properties, that we find is recruited to the latent HIV-1 promoter in a SMYD2-dependent manner. We propose that a new SMYD2-H4K20me1-L3MBTL1 axis contributes to HIV-1 latency and can be targeted with small-molecule SMYD2 inhibitors.

Introduction

Therapeutic targeting of the enzymes that deposit repressive histone marks, such as histone deacetylases (HDACs), is a promising strategy to clinically reverse HIV latency (Archin et al., 2012). Viral latency is established early after infection mostly in long-lived resting $CD4^+$ memory T cells due to the persistence of transcriptionally silenced HIV provirus (Murray et al., 2016). From here, the virus can spontaneously reactivate and, thus, rekindle infection when highly active antiretroviral therapy (HAART) is stopped. To eliminate viral reservoirs, one strategy focuses on reversing HIV latency via "shock and kill" (Deeks, 2012). The basis of this strategy is to overcome the molecular mechanisms of HIV latency by therapeutically inducing viral gene and protein expression under the protection of HAART and to cause selective cell death via the lytic properties of the virus or the immune system now recognizing the infected cells. Naturally, latent HIV is reactivated by activation of the infected T cell through the T-cell receptor or via soluble factors (i.e., cytokines such as TNFα), which activate cellular transcription factor binding to the integrated HIV provirus and initial viral transcript production (Folks et al., 1989) . This leads to *de novo* production of the virally encoded transactivator Tat, which among other functions recruits the positive transcription elongation factor b (P-TEFb) to the 5′ ends of viral transcripts to potently enhance viral transcription via the cellular RNA polymerase II complex (Ott et al., 2011).

In addition, transcription of the integrated HIV genome is subject to the regulatory effects of chromatin (Easley et al., 2010). After integration into the host chromatin, an array of five nucleosomes is precisely positioned at the HIV-1 promoter located in the 5′ long terminal repeat (LTR) independently from the integration site (Verdin et al., 1993, Sheridan et al., 1997).

Downstream of the start of transcription is nucleosome-1 (nuc-1), a nucleosome encompassing the region -3 to +141 (with respect to the transcription start site). Upon activation from latency, nuc-1 is the only nucleosome to be rapidly remodeled, suggesting that its presence contributes to post-integration latency (Van Lint et al., 1996). How the HIV promoter is remodeled upon activation is not entirely clear, but it is assumed that chromatin-remodeling complexes and post-translational modifications of histones play key roles.

HDAC inhibitors were first shown to experimentally reverse HIV latency in 1996 (Van Lint et al., 1996) and have since been tested in several clinical studies (Rasmussen et al., 2016). However, their therapeutic effects so far are modest and attenuated after multiple applications (Rasmussen et al., 2016). Thus, new complementary epigenetic strategies are needed to achieve durable reactivation. Recently, the latency-reversing potential of pharmacologic inhibition of members of the BET family of human bromodomain proteins has emerged, a class of well-conserved transcriptional regulators that are distinguished by the presence of tandem bromodomains and a so-called extraterminal (ET) domain (Nicodeme et al., 2010, Filippakopoulos et al., 2010). Bromodomains bind acetylated lysines, and BET inhibitors (i.e., JQ1, I-BET) bind into the acetyl-lysine binding pocket of the bromodomains of BET proteins disrupting acetyl-lysine:bromodomain interactions and activating HIV from latency (Archin and Margolis, 2014).

Besides bromodomain inhibition and histone deacetylation, lysine methylation has emerged as a central epigenetic mechanism to regulate HIV latency (Mbonye and Karn, 2014). Proteins can be post-translationally modified by the transfer of one, two, or three methyl groups to the side chains of lysines, a process mediated by different enzymes and resulting in different, potentially

opposing transcriptional outcomes when added to the same lysine. So far, three lysine methyl transferases (KMTs) associate with the latent proviral promoter: SUV39H1, G9a, and EZH2 (Du Chene et al., 2007, Friedman et al., 2011, Imai et al., 2010). EZH2 trimethylates histone H3 lysine 27 (H3K27me3) and is a component of the polycomb repressive complex 2 (PRC2), an important mediator of facultative heterochromatin formation (Jamieson et al., 2016). Di- and trimethylation of lysine 9 at histone H3 (H3K9me2/3) is mediated by G9a and SUV39H1 activity, respectively, which stabilizes constitutive heterochromatin structures by recruiting HP1 chromodomain-containing adaptor proteins (Du Chene et al., 2007).

Because of the growing importance of lysine methylation in disease development, specifically cancer (Song et al., 2016), and intensified efforts to develop specific pharmacological inhibitors, we developed an unbiased shRNA screen of human lysine methyltransferases to test for latency reversal in infected T-cell lines. We found that knockdown of SMYD2 reproducibly and robustly activated HIV from latency, identifying SMYD2 as a new potential transcriptional repressor. SMYD2 is a member of the SMYD family of five methyltransferases. SMYD1–5 contain a catalytic SET domain that is split by a zinc finger that contains the myeloid translocation protein-8, Nervy, and DEAF-1 (MYND) motif followed by a cysteine-rich post-SET domain (Brown et al., 2006). SMYD2 regulates transcription by methylating histone 3 lysine 36 (H3K36) and histone 3 lysine 4 (H3K4), functioning as a repressor or activator, respectively, depending on the presence of heat shock protein 90 (HSP90) (Brown et al., 2006, Abu-Farha et al., 2008). Further, SMYD2 inhibits p53 function by methylating lysine 370 (K370) (Huang et al., 2006). In addition, SMYD2 methylates K810 and K860 of the retinoblastoma (RB) tumor suppressor, as well as the estrogen receptor α (ERα), poly(ADP-ribose) polymerase 1 (PARP1), and HSP90 (Cho et al., 2012, Saddic et al., 2010, Jiang et al., 2014, Zhang et al., 2013, Piao et al., 2014,

Abu-Farha et al., 2011). And recently, BTF3, PDAP1, AHNAK, and AHNAK2 were identified to be methylated by SMYD2 (Olsen et al., 2016).

Here we connect SMYD2 with HIV-1 latency and a new histone mark, monomethylated lysine 20 in histone H4 (H4K20me1). We also provide first evidence that pharmacological SMYD2 inhibition may contribute to therapeutic latency reversal pursued in a “shock-and-kill” strategy.

RESULTS

ShRNA screen identifies novel KMTs involved in HIV-1 latency

To identify novel epigenetic regulators of HIV latency, we screened small hairpin RNAs (shRNAs) that target 31 cellular KMTs in the $CD4^+$ J-Lat 5A8 cell line harboring a latent full-length HIV provirus with the fluorescent marker GFP inserted into the *nef* open-reading frame to allow monitoring of transcriptional activity by flow cytometry (**Figure 1a**) (Chan et al., 2013). HIV transcription can be induced in this cell line with αCD3/28 antibodies mimicking T cell-receptor engagement. The line also closely clustered with patient-derived cells in a recent study comparing different latency reversing agents (LRAs) in distinct models of HIV latency (Spina et al., 2013). Cells were transduced with lentiviral vectors expressing two different shRNAs targeting each KMT or a scrambled control, followed by puromycin treatment to select successfully transduced cells. Cells were then stimulated with a suboptimal or saturating dose of αCD3/28 antibodies or were left unstimulated for 24 hours, followed by flow cytometry of GFP. A particular KMT was of interest if its knockdown resulted in a difference in GFP^+ cells that was at least -0.5- or +1.5-fold relative to the scrambled control. Phenotypes that emerged were transcriptional activation that occurred spontaneously or in synergy with αCD3/28 stimulation (red) and transcriptional repression (blue) (**Figure 1b**). For five KMTs, the screen was not conclusive, as one shRNA activated and one inhibited the response (grey) (**Figure 1b**). For 9 KMTs, shRNA treatment induced no notable changes (**Supplemental Table 1**).

We identified four KMTs as repressors of HIV latency, as their knockdown with both shRNAs induced transcriptional activation (ASH1L, SMYD2, SUV39H1, and SUV420H1). EZH1, a component of the PRC2 complex linked to HIV latency (Friedman et al., 2011), showed

hyperactivation only after high-dose αCD3/28 treatment. Twelve KMTs were identified as coactivators of the reactivation response, including SET7/9, which we previously identified as a transcriptional activator of HIV that methylates the viral transactivator Tat (Pagans et al., 2010). To independently confirm repressive activities of ASH1L, SMYD2, SUV39H1, and SUV420H1, we repeated the screen in two other J-Lat clones, A72 and A2. These clones contain HIV minigenomes composed of just the HIV promoter in the 5′LTR that drives GFP expression (LTR-GFP; A72) or an LTR-Tat-IRES-GFP cassette where transcriptional activity is driven by the viral transactivator Tat (A2) (Jordan et al., 2001, Jordan et al., 2003). In both cells lines, we observed spontaneous latency reversal (≥2x increase in GFP^+ cells) in cells lacking SMYD2, ASH1L, SUV420H1, and SUV39H1, with SMYD2 representing the top hit in both cell lines (**Figure 1c**). These data identified SMYD2 as a potential new transcriptional repressor of HIV transcription in three different cell lines using two independent shRNAs. They further indicate that the repressive effect of SMYD2 is independent from the viral transactivator Tat as reactivation was also observed in the absence of Tat in A72 cells.

Inhibition of SMYD2 reactivates HIV-1 from latency

Because of SMYD2's role in p53 and RB tumor suppressor inactivation and cancer development (Huang et al., 2006, Hamamoto et al., 2015), AstraZeneca developed a specific SMYD2 inhibitor (AZ505) (Ferguson et al., 2011). AZ505 is a substrate-competitive inhibitor that binds the peptide-binding groove of the enzyme with a calculated K_d of 0.5 μM, approximately sevenfold lower than the p53 peptide. AZ505 is not cell-penetrable, but subsequent efforts identified a novel series of potent, cell-permeable SMYD2 inhibitors, including analogs AZ506 (IC_{50} = 0.017μM) and AZ391(IC_{50} = 0.027μM) (Cowen, 2013, Throner, 2015). We tested the ability of

these compounds to reverse HIV latency in the J-Lat A72 cell line. Indeed, both compounds, but not AZ505, activated GFP expression at high concentrations (5 and 10 μM), with AZ391 inducing up to 30% GFP^+ cells similar to the activity of TNFα or the BET inhibitor JQ1 (**Figure 2a**). AZ391 reduced cell viability and increased cytotoxicity and caspase-3/7 activity at concentrations above 5 μM (**Supplemental Figure S2)**, consistent with the model that inhibiting SMYD2 strengthens the pro-apoptotic properties of p53 or RB in tumor cells. When AZ391 was combined with increasing amounts of LRAs (JQ1; SAHA-an HDAC inhibitor; ingenol 3,20-dibenzoate-a protein kinase C agonist), we observed more than additive effects with JQ1, less with SAHA and practically no combination effect with ingenol 3,20-dibenzoate (**Supplemental Figure S1a**). Positive effects of AZ391 in combination with JQ1 were also observed in *ex vivo* infected human lymphocyte aggregate cultures (HLAC) from tonsils spin-infected with high concentrations of an HIV-luciferase reporter virus as described (Kutsch et al., 2002) (**Supplemental Figure S1b–f**).

Next, we tested AZ391 in $CD4^+$ T cells from HIV-1-infected individuals on suppressive ART. Four HIV-1-infected individuals, who met the criteria of suppressive ART, which is undetectable plasma HIV-1 RNA levels (<50 copies/ml) for a minimum of six months, and a $CD4^+$ T cell count of at least 350 cells/mm^3, were enrolled (**Supplemental Table 2**). In a pilot experiment, five million purified $CD4^+$ T cells from one individual were treated *ex vivo* with increasing, non-toxic concentrations of AZ391 (maximal 500 nM), JQ1 or a combination of both, or vehicle alone. After 48 hours, levels of intracellular HIV-1 mRNA were measured by droplet digital RT-PCR using a previously published primer/probe set (Laird et al., 2015). AZ391 treatment increased intracellular HIV-1 mRNA levels in a dose-dependent manner to a similar extent as JQ1; however, no additive or synergistic effects between both drugs were observed (**Figure 2b**).

This was confirmed in the three additional donors, whose $CD4^+$ T cells all responded to AZ391 (500 nM) with increased intracellular HIV-1 mRNA levels to similar levels as JQ1 (mean increases of 1.5–10-fold) (**Figure 2e**). No synergy with JQ1 was observed (not shown). In all experiments, activation with αCD3/αCD28 antibodies was included as a positive control, which elevated levels of intracellular HIV-1 mRNA between 2.7 and 40-fold (**Figure 2b/e**). No increase in global T-cell activation (**Figure 2c/f**) and no impact on cell viability were observed in response to AZ391 treatment at the indicated concentrations (**Figure 2d/g**). These results underscore SMYD2's repressive role in HIV-1 latency across different cell models and also point to marked differences in reactivity to AZ391 in combination with JQ1 between cell lines and tonsil-derived T cells versus blood-derived resting T cells from aviremic individuals. Like with other epigenetic drugs, relief of SMYD2-mediated histone restriction is insufficient to mediate full proviral reactivation in patient-derived $CD4^+$ T cells, and combinations with other LRAs will be needed to induce maximal activation in patient cells.

SMYD2 associates with the HIV promoter in cells

We next used ChIP experiments to examine SMYD2's association with the latent HIV promoter. Chromatin was prepared from J-Lat A72 cells, either unstimulated or stimulated with TNFα, incubated with a ChIP-grade SMYD2 or IgG control antibodies, and immunoprecipitated as described (Schroder et al., 2013). DNA extracted from the immunoprecipitated material or the input control, and quantitative PCR analysis was performed with primers specific for the region within the HIV promoter occupied by nuc-1 or for the irrelevant Axin2 gene (Kaehlcke et al., 2003). Significant enrichment over the input and the IgG control was observed for SMYD2 at the HIV LTR, but not at the Axin2 gene, demonstrating specific association of SMYD2 with the

latent promoter (**Figure 3a**, red bars). After TNFα activation, recruitment was reversed, consistent with a model that the repressive activity of SMYD2 was displaced when latency was reversed (**Figure 3a**, blue bars). The opposite was observed when experiments were performed with antibodies specific for the NF-κB RelA subunit, a factor recruited to the HIV promoter in response to TNFα treatment (**Figure 3a**) (Williams et al., 2006). Similar results were obtained in the A2 cell line (**Supplemental Figure S3a**). Upon knockdown of SMYD2, the ChIP signal for SMYD2 was lost at the HIV promoter, but no change was observed at the Axin2 gene, confirming the specificity of the results (**Figure 3b**). Collectively, our data identify SMYD2 as a new repressor of HIV transcription reversibly associated with the latent HIV promoter.

SMYD2 monomethylates lysine 20 in histone 4

To identify the target for SMYD2 at the latent HIV promoter, we performed *in vitro* methylation assays with recombinant SMYD2 and radio-labeled S-adenosyl methionine (SAM) on purified human histones. We noticed that histone H4 was prominently methylated by SMYD2 (**Figure 4a**). This result was surprising, because histone H3 (H3K4 and H3K36) had been identified as the main SMYD2 target (Brown et al., 2006, Abu-Farha et al., 2008). However, Wu et al. showed in a radiometric assay that histone H4 is a more efficient substrate for SMYD2 with a specific activity 3–5-fold higher than histone H3 (Wu et al., 2011). We confirmed this finding with recombinant human histone H4, which was avidly methylated by SMYD2, a process inhibited by AZ391 (**Figure 4b**). To map the site of methylation in histone H4, we used two short, synthetic histone H4 peptides (amino acids (aa) 1–21 and aa 15–24) and subjected them to *in vitro* methylation assays. Both peptides were efficiently methylated by SMYD2, a process suppressed by the addition of AZ391 (**Figure 4c**). Both peptides contain lysines K16 and K20.

The mono-, di- and trimethylated states of K20 are well known (Van Nuland and Gozani, 2016), while K16 is known to be acetylated, and was only recently found to be also methylated in a comprehensive mass spectrometry study (Tan et al., 2011). K20 methylation states are catalyzed by different enzymes with SETD8 known to be a monomethyltransferase for H4K20 and SUV420H1/2 acting as K20 di- and trimethyltransferases (Beck et al., 2012). SMYD2 is known mainly as a monomethyltransferase although dimethylation of H3K36 by SMYD2 has been reported (Brown et al., 2006).

To determine if K20 is the site of methylation in H4, we performed *in vitro* methylation assays with a K20A-mutated histone H4 peptide. K20 was efficiently methylated by SMYD2 in the wildtype peptide, a process abolished by the H4K20A mutation (**Figure 4d**). Similarly, we performed *in vitro* methylation assays with a catalytically dead SMYD2 methyltransferase (Y240F) (Saddic et al., 2010), which methylated histone H4 with substantially decreased efficiency and failed to methylate the histone H4 peptide (**Figure 4e**). To further validate H4K20 methylation by SMYD2 in the context of full-length H4 protein, we performed *in vitro* methylation reactions with histone H4 using non-radiolabeled SAM and subjected them to a LS/MS analysis. This analysis confirmed monomethylation of K20 (**Figure 4f/g/h).** No methylation of K16 was detected.

As antibodies against the different methylated states of H4K20 are readily available, we next performed ChIP analysis in A72 cells followed by qPCR specific for the HIV promoter. We found that, like SMYD2, H4K20me1, but not H4K20me2/3, was markedly enriched at the latent HIV promoter (**Figure 5a**, left panel). Upon treatment with TNFα, the H4K20me1 mark decreased, and H4K20me2/3 marks increased, consistent with a model in which H4K20me1 is

associated with suppressed and H4K20me2/3 with activated HIV transcription. Importantly, the known suppressive mark associated with SMYD2 activity, H3K36me2, was unchanged after TNFα treatment at the HIV-1 LTR while H3K4me1 was enhanced in accordance with its reported function in transcriptional activation (Abu-Farha et al., 2008) (**Supplemental Figure S4a**). Levels of histone H4 changed only minimally upon activation, and we obtained comparable results when values were normalized to total H4 levels (**Figure 5a**, right panel).

Next, we performed ChIP analysis in SMYD2 knockdown A72 cells. SMYD2 knockdown was confirmed by western blotting, α-Tubulin was used as loading control (**Supplemental Figure S4b**). Importantly, H4K20me1 was sevenfold lower after treatment with SMYD2 shRNAs than with control shRNA–treated cells, further supporting the model that SMYD2 acts as an H4K20 monomethyltransferase at the latent HIV promoter (**Figure 5b**). SMYD2 knockdown did not change expression levels of SETD8, the known monomethyltransferase for H4K20, underscoring that SMYD2 methylates H4K20 directly rather than acting indirectly via SETD8 (**Supplemental Figure S4c**). Collectively, these data identify H4K20me1 as a new histone mark associated with HIV-1 latency and implicate SMYD2 as a new H4K20 monomethyltransferase at the latent HIV LTR.

Recruitment of reader protein L3MBTL1 to the latent HIV-1 promoter

L3MBTL1 is an MBT (malignant brain tumor) family member, a highly conserved group of 11 proteins characterized by multiple MBT domains that together bind mono- and dimethylated histones (Bonasio et al., 2010). H4K20me1/2 was identified as a docking site for L3MBTL1 in chromatin by the Reinberg laboratory, who also documented chromatin-compacting properties for purified L3MBTL1 on reconstituted nucleosomal arrays (Trojer et al., 2007). To determine if

the chromatin-compacting activity of L3MBTL1 is recruited to the latent HIV promoter, we performed ChIP experiments with L3MBTL1 antibodies and found L3MBTL1 enriched at latent and disenriched at the TNFα-activated HIV promoter in A72 (**Figure 6a**) and A2 cells (**Figures 6b**). Importantly, upon knockdown of SMYD2, L3MBTL1 was dissociated from the latent HIV promoter, supporting a model where SMYD2's methyltransferase activity on H4K20 is required to recruit L3MBTL1 to the latent HIV promoter (**Figure 6c**). In support of the model that L3MBTL1 is involved in HIV-1 latency, we observed a doubling in basal transcriptional activity in A72 J-Lat cells treated with the L3MBTL1 inhibitor UNC926 (Herold et al., 2012) (**Supplemental Figure S5a,b**). Similarly, L3MBTL1 knockdown in A72 J-Lat reproducibly activated HIV-1 transcription (**Supplemental Figure S5c–e)**. These data provide a conceptual framework how SMYD2, by recruiting H4K20me1 and L3MBTL1, could lead to compaction of the HIV locus, thus contributing to durable silencing of the latent provirus.

DISCUSSION

Here, we report that treatment with a new small-molecule SMYD2 inhibitor AZ391 or shRNA-mediated knockdown of SMYD2 activates HIV-1 transcription in latently infected T-cell lines and primary T cells. We also provide evidence that SMYD2 acts as a novel monomethyltransferase for H4K20 at the latent HIV1-LTR. By ChIP, we found SMYD2, H4K20me1, and the H4K20me1-"reader" protein L3MBTL1 enriched at the latent HIV-1 promoter and displaced in response to stimulation with TNFα, consistent with a repressive epigenetic function of this new triad. These findings provide the basis for a model wherein SMYD2 induces chromatin compaction at the HIV-1 locus by monomethylating H4K20me and recruiting L3MBTL1 to the HIV-1-LTR, thereby contributing to durable silencing of the latent provirus (**Figure 7a**). We speculate this process is reversed after activation with TNFα, when SMYD2 is dissociated from the HIV promoter, or treatment with AZ391, when SMYD2's catalytic activity is inhibited (**Figure 7b**).

The H4K20me1 mark is a previously unidentified post-translational modification of latent HIV-1 LTR chromatin. While H3K27me3 and H3K9me2/3 marks have been linked to HIV-1 latency and have known ties to heterochromatin formation, an association of H4K20me1 with HIV-1 latency was initially surprising. H4K20me1/2 are involved in DNA replication and DNA damage repair, whereas H4K20me3 is a mark of silenced heterochromatic regions (Van Nuland and Gozani, 2016). However, H4K20me1 regulates cell-cycle progression where its levels decline during G1 phase, resulting in very low levels of H4K20me1 in the beginning of S phase. It accumulates during S and G2 phases, resulting in a peak in M phase (Pesavento et al., 2008, Oda et al., 2009). Therefore, H4K20me1 possibly plays an important role in chromatin structure

regulation as chromatin undergoes a high degree of compaction during G2 and M phase to prepare for division. The effect of H4K20me1 on chromatin structure during transcription and the question whether this effect is tied to the cell cycle are so far unclear. Our data indicate that the high abundance of H4K20me1 at the latent HIV promoter could serve as recruitment signal for L3MBTL1 to the integrated HIV-1 promoter where it could locally induce chromatin compaction to silence transcription. Whether HIV-1 specifically hijacks this mechanism for its own silencing or whether this is a wide-spread mechanism to silence cellular genes is under investigation.

H4K20 is a so far unrecognized histone target for SMYD2 although previous work pointed to histone H4 as a more efficient substrate for SMYD2 than histone H3 (Wu et al., 2011). Recently, Olsen et al. reported in a large-scale proteomic study of lysine monomethylation by SMYD2 H4K20me1 to be down-regulated in four of seven cell lines by both shRNA-mediated knockdown and use of a SMYD2 inhibitor, which points to a more general function of SMYD2 in H4K20 monomethylation (Olsen et al., 2016). Expression of the known H4K20 monomethyltransferase SETD8 (also known as PR-SET7) is highly regulated in the cell cycle, mirroring the dynamics of H4K20me1 occurrence (Fang et al., 2002, Nishioka et al., 2002, Schotta et al., 2004, Schotta et al., 2008). While our data using AZ391 indicate that the catalytic activity of SMYD2 is important for its latency-inducing effects, we cannot rule out that SMYD2 could, for example, methylate SETD8 at the latent HIV-1 promoter to induce SETD8-mediated monomethylation of H4K20. Similarly, SMYD2 could methylate another histone site, which then could activate H4K20 monomethylation by SETD8. It is, however, important to point out that SETD8 knockdown in the present RNAi screen had the opposite effect on HIV-1 latency than knockdown of SMYD2. SETD8 was identified as a coactivator of HIV transcription as

knockdown suppressed latency reactivation, thus excluding SETD8 as a mediator of the repressive SMYD2 function at the latent HIV LTR (**Figure 1b**).

Posttranslational modifications are recognized by so-called “reader” proteins that bind to modified residues via specialized binding modules (Patel and Wang, 2013). H4K20me1 is recognized by L3MBTL1, a process that leads to chromatin compaction and thus transcriptional silencing (Trojer et al., 2007, Min et al., 2007, Kalakonda et al., 2008). L3MBTL2 is a member of the PRC1 complex, and L3MBTL1 has common binding partners with RING1B, the catalytic subunit of the PRC1 complex, possibly linking L3MBTL1 to PRC1, another factor independently associated with chromatin compaction (Trojer et al., 2011, Francis et al., 2004). A possible link between L3MBTL1 and SMYD2 was suggested by Saddic et al., who showed that RB can bind directly to the 3xMBT domain of L3MBTL1, which is facilitated by SMYD2-mediated RB methylation at Lys-860 (Saddic et al., 2010). Saddic et al. suggested a model whereby RB methylation by SMYD2 recruits L3MBTL1 to the promoters of specific RB/E2F target genes to repress their transcription (Saddic et al., 2010). One report shows E2F1-mediated suppression of the LTR activity in transient transfection experiments (Kundu et al., 1995), indicating that SMYD2 could recruit L3MBTL1 to the latent HIV-1 LTR also through possible engagement of RB/E2F1, independently from H4K20me1.

The different effect of BET and SMYD2 inhibitor combinations on HIV-1 latency reversal in distinct cells systems is intriguing and requires further investigation. Similarly, it is surprising that protein kinase C activation did not synergize with SMYD2 inhibition as it was shown for HDAC or BET inhibitors (Archin and Margolis, 2014), suggesting a fundamental difference between manipulation of protein acetylation and methylation in this respect. In a first evaluation,

we found that BET inhibition through JQ1 decreases expression of SMYD2 mRNA in cell lines, pointing to a regulation of SMYD2 transcription by BET proteins, including BRD4 (not shown). Recently, SMYD2 was shown to be transcriptionally regulated by the oncogenic transcription factor MYC (Bagislar et al., 2016), a transcription factor primarily targeted by JQ1 treatment (Delmore et al., 2011). As MYC activity is likely different in cell lines, partially activated tonsil-resident T cells and resting blood circulating T cells (Wang et al., 2011), we speculate that this difference may explain the differential response to a JQ1-AZ391 combination treatment in these cell types. These and other possibilities need to be further pursued in future experiments.

In summary, our findings show that SMYD2 has a previously unrecognized silencing role in latent HIV transcription and link this role with H4K20 monomethylation and L3MBTL1 recruitment at the latent HIV LTR. In addition, they uncover a potential novel therapeutic approach in HIV latency reversal via pharmacological SMYD2, underscoring the emerging ties between cancer and HIV treatment through shared epigenetic drug targets.

AUTHOR CONTRIBUTIONS

Conceptualization, D.B. and M.O.; Methodology, D.B. and M.O.; Investigation, D.B., M.J., G.C., A.G., R.S., J.R.J., P.A.H., N.S., S.P. and M.M.; Writing – Original Draft, D.B. and M.O.; Writing Review & Editing, D.B. and M.O.; Funding Acquisition, D.B., W.C.G. and M.O.; Resources, R.G. and S.G.D.; Supervision, N.J.K., W.C.G. and M.O..

ACKNOWLEDGEMENTS

We thank members of the Ott, Miranda, Greene, and Verdin laboratories for helpful discussions, reagents and expertise. For help with the shRNA screen we thank Amy Wong, a student intern from the Gladstone Promoting Underrepresented Minorities Advancing in the Sciences (PUMAS) internship program. We thank John Carroll and Teresa Roberts for graphics, Gary Howard for editorial and Veronica Fonseca for administrative assistance. This publication was made possible with the help from the University of California, San Francisco–Gladstone Institute of Virology & Immunology Center for AIDS Research (P30 AI027763) and amfAR Institute for HIV Cure Research, with funding from amfAR grant number 109301. We gratefully acknowledge support from the California HIV/AIDS Research Program (Award number: F13-GI-316) to D.B., the James B. Pendleton Charitable Trust, and an industry-sponsored collaboration with JT Pharma to M.O. as well as grant support from the CARE Collaboratory (U19 AI096113) to M.O. and W.C.G., the NIH (RO1 AI083139 and RO1 DA043142) to M.O. and (P50 GM082250) to N.J.K.

CONFLICT OF INTEREST

The authors declare no conflicts of interest.

378

REFERENCES

Abu-Farha, M., et al. 2008. The tale of two domains: proteomics and genomics analysis of SMYD2, a new histone methyltransferase. *Mol Cell Proteomics,* 7**,** 560-72.

Abu-Farha, M., et al. 2011. Proteomic analyses of the SMYD family interactomes identify HSP90 as a novel target for SMYD2. *J Mol Cell Biol,* 3**,** 301-8.

Archin, N. M., et al. 2012. Administration of vorinostat disrupts HIV-1 latency in patients on antiretroviral therapy. *Nature,* 487**,** 482-5.

Archin, N. M. & Margolis, D. M. 2014. Emerging strategies to deplete the HIV reservoir. *Curr Opin Infect Dis,* 27**,** 29-35.

Bagislar, S., et al. 2016. Smyd2 is a Myc-regulated gene critical for MLL-AF9 induced leukemogenesis. *Oncotarget,* 7**,** 66398-66415.

Beck, D. B., et al. 2012. PR-Set7 and H4K20me1: at the crossroads of genome integrity, cell cycle, chromosome condensation, and transcription. *Genes Dev,* 26**,** 325-37.

Bonasio, R., et al. 2010. MBT domain proteins in development and disease. *Semin Cell Dev Biol,* 21**,** 221-30.

Brown, M. A., et al. 2006. Identification and characterization of Smyd2: a split SET/MYND domain-containing histone H3 lysine 36-specific methyltransferase that interacts with the Sin3 histone deacetylase complex. *Mol Cancer,* 5**,** 26.

Chan, J. K., et al. 2013. Calcium/calcineurin synergizes with prostratin to promote NF-kappaB dependent activation of latent HIV. *PLoS One,* 8**,** e77749.

Cho, H. S., et al. 2012. RB1 methylation by SMYD2 enhances cell cycle progression through an increase of RB1 phosphorylation. *Neoplasia,* 14**,** 476-86.

Cowen, S. D. Targeting the Substrate Binding Site of Methyl Transferases; Structure Based Design of SMYD2 Inhibitors. EpiCongress 2013, Boston, MA, July 23-24, 2013., 2013.

Cox, J. & Mann, M. 2008. MaxQuant enables high peptide identification rates, individualized p.p.b.-range mass accuracies and proteome-wide protein quantification. *Nat Biotechnol,* 26**,** 1367-72.

Deeks, S. G. 2012. HIV: Shock and kill. *Nature,* 487**,** 439-40.

Delmore, J. E., et al. 2011. BET bromodomain inhibition as a therapeutic strategy to target c-Myc. *Cell,* 146**,** 904-17.

Du Chene, I., et al. 2007. Suv39H1 and HP1gamma are responsible for chromatin-mediated HIV-1 transcriptional silencing and post-integration latency. *EMBO J,* 26**,** 424-35.

Easley, R., et al. 2010. Chromatin dynamics associated with HIV-1 Tat-activated transcription. *Biochim Biophys Acta,* 1799**,** 275-85.

Fang, J., et al. 2002. Purification and functional characterization of SET8, a nucleosomal histone H4-lysine 20-specific methyltransferase. *Curr Biol,* 12**,** 1086-99.

Ferguson, A. D., et al. 2011. Structural basis of substrate methylation and inhibition of SMYD2. *Structure,* 19**,** 1262-73.

Filippakopoulos, P., et al. 2010. Selective inhibition of BET bromodomains. *Nature,* 468**,** 1067-73.

Folks, T. M., et al. 1989. Tumor necrosis factor alpha induces expression of human immunodeficiency virus in a chronically infected T-cell clone. *Proc Natl Acad Sci U S A,* 86**,** 2365-8.

Francis, N. J., et al. 2004. Chromatin compaction by a polycomb group protein complex. *Science,* 306**,** 1574-7.
Friedman, J., et al. 2011. Epigenetic silencing of HIV-1 by the histone H3 lysine 27 methyltransferase enhancer of Zeste 2. *J Virol,* 85**,** 9078-89.
Hamamoto, R., et al. 2015. Critical roles of non-histone protein lysine methylation in human tumorigenesis. *Nat Rev Cancer,* 15**,** 110-24.
Herold, J. M., et al. 2012. Structure-activity relationships of methyl-lysine reader antagonists. *Medchemcomm,* 3**,** 45-51.
Huang, J., et al. 2006. Repression of p53 activity by Smyd2-mediated methylation. *Nature,* 444**,** 629-32.
Imai, K., et al. 2010. Involvement of histone H3 lysine 9 (H3K9) methyltransferase G9a in the maintenance of HIV-1 latency and its reactivation by BIX01294. *J Biol Chem,* 285**,** 16538-45.
Jamieson, K., et al. 2016. Loss of HP1 causes depletion of H3K27me3 from facultative heterochromatin and gain of H3K27me2 at constitutive heterochromatin. *Genome Res,* 26**,** 97-107.
Jiang, Y., et al. 2014. Structural insights into estrogen receptor alpha methylation by histone methyltransferase SMYD2, a cellular event implicated in estrogen signaling regulation. *J Mol Biol,* 426**,** 3413-25.
Jordan, A., et al. 2003. HIV reproducibly establishes a latent infection after acute infection of T cells in vitro. *Embo J,* 22**,** 1868-77.
Jordan, A., et al. 2001. The site of HIV-1 integration in the human genome determines basal transcriptional activity and response to Tat transactivation. *EMBO J,* 20**,** 1726-38.
Kaehlcke, K., et al. 2003. Acetylation of Tat defines a cyclinT1-independent step in HIV transactivation. *Mol Cell,* 12**,** 167-76.
Kalakonda, N., et al. 2008. Histone H4 lysine 20 monomethylation promotes transcriptional repression by L3MBTL1. *Oncogene,* 27**,** 4293-304.
Kundu, M., et al. 1995. Evidence that a cell cycle regulator, E2F1, down-regulates transcriptional activity of the human immunodeficiency virus type 1 promoter. *J Virol,* 69**,** 6940-6.
Kutsch, O., et al. 2002. Direct and quantitative single-cell analysis of human immunodeficiency virus type 1 reactivation from latency. *J Virol,* 76**,** 8776-86.
Laird, G. M., et al. 2015. Ex vivo analysis identifies effective HIV-1 latency-reversing drug combinations. *J Clin Invest,* 125**,** 1901-12.
Maclean, B., et al. 2010. Skyline: an open source document editor for creating and analyzing targeted proteomics experiments. *Bioinformatics,* 26**,** 966-8.
Mbonye, U. & Karn, J. 2014. Transcriptional control of HIV latency: cellular signaling pathways, epigenetics, happenstance and the hope for a cure. *Virology,* 454-455**,** 328-39.
Min, J., et al. 2007. L3MBTL1 recognition of mono- and dimethylated histones. *Nat Struct Mol Biol,* 14**,** 1229-30.
Murray, A. J., et al. 2016. The Latent Reservoir for HIV-1: How Immunologic Memory and Clonal Expansion Contribute to HIV-1 Persistence. *J Immunol,* 197**,** 407-17.
Naldini, L., et al. 1996. In vivo gene delivery and stable transduction of nondividing cells by a lentiviral vector. *Science,* 272**,** 263-7.
Nicodeme, E., et al. 2010. Suppression of inflammation by a synthetic histone mimic. *Nature,* 468**,** 1119-23.

Nishioka, K., et al. 2002. PR-Set7 is a nucleosome-specific methyltransferase that modifies lysine 20 of histone H4 and is associated with silent chromatin. *Mol Cell,* 9**,** 1201-13.

Oda, H., et al. 2009. Monomethylation of histone H4-lysine 20 is involved in chromosome structure and stability and is essential for mouse development. *Mol Cell Biol,* 29**,** 2278-95.

Olsen, J. B., et al. 2016. Quantitative Profiling of the Activity of Protein Lysine Methyltransferase SMYD2 Using SILAC-Based Proteomics. *Mol Cell Proteomics,* 15**,** 892-905.

Ott, M., et al. 2011. The control of HIV transcription: keeping RNA polymerase II on track. *Cell Host Microbe,* 10**,** 426-35.

Pagans, S., et al. 2010. The Cellular lysine methyltransferase Set7/9-KMT7 binds HIV-1 TAR RNA, monomethylates the viral transactivator Tat, and enhances HIV transcription. *Cell Host Microbe,* 7**,** 234-44.

Patel, D. J. & Wang, Z. 2013. Readout of epigenetic modifications. *Annu Rev Biochem,* 82**,** 81-118.

Pesavento, J. J., et al. 2008. Certain and progressive methylation of histone H4 at lysine 20 during the cell cycle. *Mol Cell Biol,* 28**,** 468-86.

Piao, L., et al. 2014. The histone methyltransferase SMYD2 methylates PARP1 and promotes poly(ADP-ribosyl)ation activity in cancer cells. *Neoplasia,* 16**,** 257-64, 264 e2.

Rafati, H., et al. 2011. Repressive LTR nucleosome positioning by the BAF complex is required for HIV latency. *PLoS Biol,* 9**,** e1001206.

Rasmussen, T. A., et al. 2016. Reversal of Latency as Part of a Cure for HIV-1. *Trends Microbiol,* 24**,** 90-7.

Saddic, L. A., et al. 2010. Methylation of the retinoblastoma tumor suppressor by SMYD2. *J Biol Chem,* 285**,** 37733-40.

Schotta, G., et al. 2004. A silencing pathway to induce H3-K9 and H4-K20 trimethylation at constitutive heterochromatin. *Genes Dev,* 18**,** 1251-62.

Schotta, G., et al. 2008. A chromatin-wide transition to H4K20 monomethylation impairs genome integrity and programmed DNA rearrangements in the mouse. *Genes Dev,* 22**,** 2048-61.

Schroder, S., et al. 2013. Acetylation of RNA polymerase II regulates growth-factor-induced gene transcription in mammalian cells. *Mol Cell,* 52**,** 314-24.

Sheridan, P. L., et al. 1997. Histone acetyltransferases regulate HIV-1 enhancer activity in vitro. *Genes Dev,* 11**,** 3327-40.

Song, Y., et al. 2016. Targeting histone methylation for cancer therapy: enzymes, inhibitors, biological activity and perspectives. *J Hematol Oncol,* 9**,** 49.

Spina, C. A., et al. 2013. An in-depth comparison of latent HIV-1 reactivation in multiple cell model systems and resting CD4+ T cells from aviremic patients. *PLoS Pathog,* 9**,** e1003834.

Tan, M., et al. 2011. Identification of 67 histone marks and histone lysine crotonylation as a new type of histone modification. *Cell,* 146**,** 1016-28.

Throner, S. C., S.; Russell, D. J.; Dakin, L.; Chen, H.; Larsen, N. A.; Godin, R. E.; Zheng, X.; Molina, A.; Wu, J.; Cheung, T.; Howard, T.; Garcia-Arenas, R.; Keen, N.; Ferguson, A. D. Abstracts of Papers,. 250th National Meeting of the American Chemical Society, , 2015 Boston, MA, Aug 16–20, 2015; American Chemical Society: Washington, DC, 2015; MEDI 513.

Trojer, P., et al. 2011. L3MBTL2 protein acts in concert with PcG protein-mediated monoubiquitination of H2A to establish a repressive chromatin structure. *Mol Cell,* 42**,** 438-50.
Trojer, P., et al. 2007. L3MBTL1, a histone-methylation-dependent chromatin lock. *Cell,* 129**,** 915-28.
Van Lint, C., et al. 1996. Transcriptional activation and chromatin remodeling of the HIV-1 promoter in response to histone acetylation. *EMBO J,* 15**,** 1112-20.
Van Nuland, R. & Gozani, O. 2016. Histone H4 Lysine 20 (H4K20) Methylation, Expanding the Signaling Potential of the Proteome One Methyl Moiety at a Time. *Mol Cell Proteomics,* 15**,** 755-64.
Verdin, E., et al. 1993. Chromatin disruption in the promoter of human immunodeficiency virus type 1 during transcriptional activation. *EMBO J,* 12**,** 3249-59.
Wang, R., et al. 2011. The transcription factor Myc controls metabolic reprogramming upon T lymphocyte activation. *Immunity,* 35**,** 871-82.
Williams, S. A., et al. 2006. NF-kappaB p50 promotes HIV latency through HDAC recruitment and repression of transcriptional initiation. *EMBO J,* 25**,** 139-49.
Wu, J., et al. 2011. Biochemical characterization of human SET and MYND domain-containing protein 2 methyltransferase. *Biochemistry,* 50**,** 6488-97.
Zhang, X., et al. 2013. Regulation of estrogen receptor alpha by histone methyltransferase SMYD2-mediated protein methylation. *Proc Natl Acad Sci U S A,* 110**,** 17284-9.

MAIN FIGURE TITLES AND LEGENDS

Figure 1: ShRNA screen identifies novel KMTs involved in HIV-1 latency. (a) Schematic representation of the screen. Two shRNAs/ gene were transfected into J-Lat 5A8 cells. After 7 days of puromycin selection, cells were treated with 0.125/1.0 µg αCD3/28 (low), and 1.0/1.0 µg αCD3/28 (high), or left untreated (basal). After 18 h, the percentages of GFP^+ cells were determined using a MACSQuant VYB FACS analyzer (Miltenyi Biotech GmbH). Analysis was conducted on 3x 10,000 live cells per condition, and the screen was independently repeated two times. Validation of shRNA knockdown was confirmed using qPCR. **(b)** Heat map of shRNA hits identified. We identified four suppressors (red) and 12 activators of HIV transcription (blue). For five KMTs, the screens were not conclusive, as one shRNA activated and one inhibited the response (grey). **(c)** Fold activation of SMYD2, ASH1L, SUV420H1, and SUV39H1 knocked down in Jurkat A2 (LTR-Tat-IRES-GFP) and A72 (LTR-GFP) J-Lat cells without co-stimulation. Analysis was conducted on 3x 10,000 live cells per condition, and all experiments were independently repeated at least three times. Cell viability (% survival) was monitored by forward and side scatter analysis. ShRNA knockdown (%KD) was confirmed using qPCR. SMYD2 knockdown reproducibly activated HIV-1 transcription spontaneously without co-stimulation.

Figure 2: Reactivation of latent HIV-1 with SMYD2 inhibitor AZ391 (a) J-Lat cell line A72 was treated with SMYD2 inhibitors AZ505, AZ506, and AZ391 at increasing concentrations (10 nM–5 µM) for 18 h and analyzed by flow cytometry. 2 ng/ml TNFα or 1 µM JQ1 were used as controls. Structures of each compound are shown above the chart. As indicated, stimulation with

AZ391 or the controls increased GFP expression. Data represent average (± SD) of three independent experiments. **(b)** Intracellular HIV-1 mRNA levels in $CD4^+$ T cells, obtained from an infected individual (#1036) and treated *ex vivo* with AZ391, JQ1 or a combination of both, in indicated concentrations, presented as fold induction relative to DMSO control. Activation with αCD3/αCD28-Dynabeads was performed as control. **(c)** Flow cytometry of T-cell activation markers CD69 (blue) and CD69 (burgundy) in the same experiment. Shown as percentage of positive cells relative to αCD3/αCD28-treated cells **(d)** Cell viability as measured by CellTiter-Blue® Cell Viability assay (Promega) and Zombie Violet Fixable Viability kit (BioLegend) and presented as percentage of DMSO control treated cells. Data points indicate average of three technical replicates of donor #1036. **(e–g)** Same experiments as in b–d but performed with $CD4^+$ T cells obtained from three additional individuals (2013, 2185, 2511) with a single concentration of AZ391 (500 nM). In f and g, average of the three biological replicates (±SD) is show.

Figure 3: SMYD2 associates with the HIV promoter in cells. Chromatin immunoprecipitation (ChIP) assays with antibodies against SMYD2, RelA, and IgG control at the HIV LTR, followed by qPCR using primers specific for HIV-1 LTR Nuc1 or Axin2. Chromatin was prepared from J-Lat A72 cells, in which the LTR was stimulated by TNFα treatment or which were left untreated. **(a)** SMYD2 is present at the HIV-LTR under non-stimulated conditions (red), and was displaced in response to TNFα stimulation (blue, left). RelA is recruited to the HIV promoter after treatment with TNFα (blue, right). No association of SMYD2 or RelA with Axin2 was observed. All chromatin immunoprecipitations and qPCRs were repeated at least three times and representative results of three technical replicates are shown. In the left panel, results are expressed as percent enrichment over input DNA values. In the right and all following ChIP panels, results are expressed as fold increase over IgG control (IgG=1). **(b)** Confirmation of

SMYD2 knockdown by qPCR in A72 J-Lat cells (left). SMYD2 is present at the HIV-LTR in scramble control cells (red) and absent in SMYD2 knockdown cells (blue, right). All ChIPs and qPCRs were repeated at least three times, and representative results of three technical replicates are shown. For statistical comparison of ChIP experiments, the difference in dis-enrichment (SMYD2) or enrichment (RelA) between control and TNFα treatment **(a)** or scramble control and shRNA treatment **(b)** was calculated and 3 biological replicates were analyzed by t-test. A value of $p < 0.05$ was considered significant.

Figure 4: SMYD2 methylates histone 4 at lysine 20. *In vitro* methylation assays, including histones isolated from HEK293T, recombinant full-length histone H4 or two short synthetic histone H4 peptides (aa 1-–21 and aa 15–24) that were incubated with recombinant SMYD2 enzyme and radiolabeled H^3-S-adenosyl-L-methionine (SAM) in the presence or absence of AZ391. Reactions were resolved by gel electrophoresis and developed by autoradiography. **(a)** *In vitro* methylation assays of histones isolated from HEK293T cells. **(b)** *In vitro* SMYD2 methylation assay of recombinant full-length histone H4, with or without AZ391. **(c)** *In vitro* SMYD2 methylation assays of synthetic histone H4 peptides (aa 1–21, left, and aa 15–24, right) in the presence or absence of AZ391. **(d)** *In vitro* SMYD2 methylation assay of synthetic histone H4 peptide (aa 1–21) with or without a K20A mutation. **(e)** *In vitro* methylation assays of human recombinant histone H4 using wildtype or catalytically inactive (Y240F) SMYD2. All *in vitro* methylation assays of recombinant histone H4 or H4 peptides were repeated at least three times, and representative Coomassie stain (left) and autoradiography (right) are shown. **(f–h)** *In vitro* SMYD2 methylation assay of recombinant full-length histone H4 was subjected to mass

spectrometry. (**f**) Annotated HCD MS/MS spectrum of the histone H4 LysC peptide RHRKmeVLRDIQGITK containing K20 methylation. Blue lines indicate b ions and purple lines indicate y ions, with specific ions labeled atop each peak. (**g–h**) Integrated MS1 intensity for the RHRKmeVLRDIQGITK peptide (**g**) and an unmodified histone H4 peptide (**h**) across different samples. Error bars indicate standard deviation between technical replicate MS analyses.

Figure 5: Deposition of H4K20me at the HIV LTR depends on SMYD2. (a) ChIP experiments performed with antibodies against H4, H4K20me, H4K20me2, and H4K20me3 at the HIV LTR, followed by qPCR using primers specific for HIV-1 LTR Nuc1 or Axin2. Chromatin was prepared from J-Lat A72 cells, in which the LTR was stimulated by TNFα treatment or which were left untreated. H4K20me1 was highly present at the uninduced HIV-LTR (red) but reduced in response to TNFα (blue). H4K20me2 increased after treatment with TNFα, while histone H4 remained unchanged. Left panel shows results relative to IgG control, and right panel shows results relative to histone H4. All ChIPs and qPCRs were repeated at least three times, and representative results of three technical replicates are shown. **(b)** ChIP experiments of histone H4 and the H4K20 methyl marks performed in SMYD2 knockdown (blue) or scrambled control cells (red). H4K20me1 is present at the uninduced HIV-LTR in the scrambled control cells (red), and decreased ~sevenfold upon SMYD2 knockdown (blue). Left panel shows results relative to IgG control and right panel shows results relative to histone H4. All ChIPs and qPCRs were repeated at least three times, and representative results of three technical replicates are shown. For statistical comparison of ChIP experiments, the difference in dis-enrichment (H4K20me) between control and TNFα treatment **(a)** or scramble control and shRNA treatment **(b)** was calculated and 3 biological replicates were analyzed by t-test. A value of $p < 0.05$ was considered significant.

Figure 6: L3MBTL1 associates with the HIV promoter in cells. (a) ChIP experiments of L3MBTL1 in A72 J-Lat cells, either non-stimulated (red) or in response to TNFα stimulation (blue) at the HIV LTR nuc-1 region (left) or at the Axin2 gene (right). All ChIPs and qPCRs were repeated at least three times, and representative results of three technical replicates are shown. **(b)** ChIP experiments of L3MBTL1 in A2 J-Lat cells, either non-stimulated (red) or in response to TNFα stimulation (blue) at the HIV LTR nuc-1 region (left) or at the Axin2 gene (right). All ChIPs and qPCRs were repeated at least three times, and representative results of three technical replicates are shown. **(c)** ChIP experiments of L3MBTL1 performed in two SMYD2 knockdown A2 cell lines (green) or scramble control cells (red). All ChIPs and qPCRs were repeated at least three times, and representative results of three technical replicates are shown. For statistical comparison of ChIP experiments, the difference in dis-enrichment (L3MBTL1) between control and TNFα treatment in A72 cells **(a),** the difference in dis-enrichment (L3MBTL1) between control and TNFα treatment in A2 cells **(b),** or scramble control and shRNA treatment **(c)** was calculated and 3 biological replicates were analyzed by t-test. A value of $p < 0.05$ was considered significant.

Figure 7: Model of SMYD2's repressive function at the latent HIV LTR. SMYD2 induces chromatin compaction at the HIV-1 locus by monomethylating H4K20me and recruiting L3MBTL1 to the HIV-1-LTR, thereby repressing transcription.

STAR METHODS

CONTACT FOR REAGENT AND RESOURCE SHARING

Further information and requests for resources and reagents should be directed to and will be fulfilled by the Lead Contact, Melanie Ott (mott@gladstone.ucsf.edu). The compounds AZ505, AZ506 and AZ391 were received by Gladstone Institutes under a Material Transfer Agreement.

EXPERIMENTAL MODEL AND SUBJECT DETAILS

Cell lines and primary cultures

Female HEK293T were obtained from the American Type Culture Collection. HEK293T cells were cultured at 37°C in DMEM supplemented with 10% fetal bovine serum (FBS) (Gemini), 1% L-glutamine (Life Technologies) and 1% penicillin-streptomycin (Life Technologies). J-Lat cell lines (clones A2, A72, and 5A8) were obtained directly from the Verdin and Greene Laboratories here at the Gladstone Institutes, which originally generated these lines from male Jurkat cells (Jordan et al., 2003, Chan et al., 2013). All cell lines are confirmed clonal, thawed from early freeze-downs, kept in culture no longer than four weeks and were regularly (every 6 months) tested for Mycoplasma contamination. J-Lat cells were cultured at 37°C in RPMI supplemented with 10% FBS, 1% L-glutamine and 1% penicillin-streptomycin. Primary CD4+ T cells were obtained from Leukoreduction Chambers from Trima Apheresis Collection from anonymous blood donors or as de-identified study participants from Dr. Deeks (SCOPE Cohort at University of California, San Francisco, **Supplemental Table 2**). Primary CD4+ T cells were isolated via negative selection without activation, and their resting status was verified by CD69, CD25 staining and flow cytometry. Primary CD4+ T cells were cultured at 37°C in RPMI

supplemented with 10% FBS, 1% L-glutamine and 1% penicillin-streptomycin. Experiments were performed in individual cell cultures isolated from 3-4 donors and results from multiple donors were averaged and compared using standard deviation (±SD).

METHOD DETAILS

ShRNA-mediated knockdown and flow cytometry

ShRNA-expressing lentiviral vectors were purchased from Sigma-Aldrich. The plasmids used in the shRNA screen are listed in **Supplemental Table 3**. The pLKO.1 vector containing a scrambled shRNA was used as control. Pseudotyped viral stocks were produced in 2 x 10^6 HEK293T cells by the calcium phosphate method by co-transfecting 10 µg of shRNA-expressing lentiviral vectors, with 6.5 µg of the lentiviral packaging construct pCMVdelta R8.91 and 3.5 µg of VSV-G glycoprotein-expressing vector (Naldini et al., 1996), and titered for p24 content. J-Lat 5A8, A72 and A2 cells were spininfected with virus (1 ng of p24 per 10^6 cells) containing shRNAs against KMTs or nontargeting control shRNAs and were selected with puromycin (2 µg/ml; Sigma). After 7 days of selection, cells were treated with the indicated concentration of drugs. The percentage of GFP^+ cells was determined after 18 h using a MACSQuant VYB FACS analyzer (Miltenyi Biotech GmbH). Cell viability was monitored by forward-and-side scatter analysis. The shRNA screen was repeated twice in 5A8 cells and analysis was conducted on 3 x 10,000 live cells per condition. Data were analyzed using FlowJo 9.9 (Tree Star). Hits from the shRNA screen where validated in A2 and A72 J-Lat cells. Three biological replicates of experiments in A2 and A72 J-Lat cells were averaged and compared using standard deviation (±SD).

Drug treatments

TNFα (Sigma-Aldrich) was used at 0.5–10 ng/ml. Human αCD3/αCD28 Dynabeads (Invitrogen) were used at a 1 bead/cell ratio. JQ1 (Cayman Chemical) was used at 0.1–10 μM. Ingenol 3,20-dibenzoate (Santa Cruz Biotechnology) was used at 5–200 nM, and SAHA (Merck) was used at 110 nM, 330 nM, or 1 μM. Phorbol 12-myristate 13-acetate (PMA) (Sigma-Aldrich) was used at 10 nM and ionomycin (Sigma-Aldrich) was used at a concentration of 500 nM. UNC926 (Tocris Bioscience) was used at a concentration of 10 nM–100 μM. AZ505, AZ506, and AZ391 were used at a concentration of 10 nM–10 μM.

RNA isolation, RT and quantitative RT-PCR

RNA was isolated using RNeasy Plus Mini Kit (Qiagen) and reverse-transcribed using SuperScript III Reverse Transcriptase (Invitrogen) as per the manufacturer's instructions. Quantitative RT-PCR was carried out using Maxima SYBR Green qPCR Master Mix (Thermo Scientific) on SDS 2.4 software (Applied Biosystems) in a total volume of 12 μL. Primer efficiencies were around 100%. Dissociation curve analysis was performed after the end of the PCR to confirm the presence of a single and specific product. All qPCRs were independently repeated at least three times, averaged and compared using standard deviation (±SD)..

Chromatin immunoprecipitation

J-Lat A2 and A72 cells were treated with TNFα (10 ng/ml) for 18 h. Cells were fixed with 1% formaldehyde (v/v) in fixation buffer (1 mM EDTA, 0.5 mM EGTA, 50 mM Hepes, pH 8.0, 100 mM NaCl), and fixation was stopped after 10 min by addition of glycine to 125 mM. The cell membrane was lysed for 15 min on ice (5 mM Pipes, pH 8.0, 85 mM KCl, 0.5% NP40, protease

inhibitors). After washing with nuclear swell buffer (25 mM HEPES, pH 7.5, 4 mM KCl, 1 mM DTT, 0.5% NP-40, 0.5 mM PMSF) and micrococcal nuclease (MNase) digestion buffer (20 mM Tris pH 7.5, 2.5 mM CaCl2, 5 mM NaCl, 1 mM DTT, 0.5 % NP-40), the pellet was resuspended in MNase buffer (15 mM Tris-HCl, pH 7.5, 5 mM MgCl2, 1 mM CaCl2, and 25 mM NaCl). Subsequently, samples were incubated with MNase (New England Biolabs) for 10 min at RT. The reaction was quenched with 0.5 M EDTA and incubated on ice for 5 min. Cells were lysed (1% SDS, 10 mM EDTA, 50 mM Tris-HCl, pH 8.1, protease inhibitors), and chromatin DNA was sheared to 200–1000-bp average size through sonication (Ultrasonic Processor CP-130, Cole Parmer). Cellular debris was pelleted, and the supernatant was recovered. Protein A/G Sepharose beads were blocked with single-stranded salmon sperm DNA and BSA, washed and resuspended in immunoprecipitation buffer. Blocked protein A/G Sepharose beads were added to the digested chromatin fractions and rotated at 4°C for 2 h to preclear chromatin. Lysates were incubated overnight at 4°C with 5 µg of SMYD2, RelA, histone H4, H4K20me1, H4K20me2, H4K20me3 antibodies, or IgG control. After incubation with protein A/G agarose beads for 2 h and washing three times with low salt buffer (0.1% SDS, 1% Triton X-100, 2 mM EDTA, 20 mM Tris-HCl, pH 8.1, 150 mM NaCl), one time with high salt buffer (0.1% SDS, 1% Triton X-100, 2 mM EDTA, 20 mM Tris-HCl, pH 8.1, 500 mM NaCl) and twice with TE-buffer (1 mM EDTA, 10 mM Tris-HCl, pH 8.1), chromatin was eluted and recovered with Agencourt AMPure XP beads (Beckman Coulter). Bound chromatin and input DNA were treated with RNase H (New England Biolabs) and Proteinase K (Sigma-Aldrich) at 37 °C for 30 min. Immunoprecipitated chromatin was quantified by real-time PCR using the Maxima SYBR Green qPCR Master Mix (Thermo Scientific) and the ABI 7700 Sequence Detection System (Applied Biosystems). The SDS 2.4 software (Applied Biosystems) was used for analysis. The specificity of each PCR reaction was

confirmed by melting curve analysis using the Dissociation Curve software (Applied Biosystems). All chromatin immunoprecipitations and qPCRs were repeated at least three times, and representative results were shown.

Primer sequences were:

HIV LTR Nuc1 forward: 5' AGTGTGTGCCCGTCTGTTGT 3',

HIV LTR Nuc1 reverse: 5' TTCGCTTTCAGGTCCCTGTT 3',

Axin2 forward 5’ GCCAGAGTCAAGCCAGTAGTC 3’ (Rafati et al., 2011)

Axin2 reverse: 5’ TAGCCTAATGTGGAGTGGATGTG 3’ (Rafati et al., 2011)

Primary CD4$^+$ T cell experiments

Four aviremic HIV-1-infected individuals were recruited from the SCOPE cohorts at the University of California, San Francisco. **Supplemental Table** 2 details the characteristics of the study participants.

Peripheral blood mononuclear cells (PBMCs) from whole blood or continuous flow centrifugation leukapheresis product were purified using density centrifugation on a Ficoll-Hypaque gradient. Resting CD4$^+$ lymphocytes were enriched by negative depletion with an EasySepHuman CD4$^+$ T Cell Isolation Kit (Stemcell). Cells were cultured in RPMI medium supplemented with 10% fetal bovine serum, penicillin/streptomycin and 5 μM saquinavir. Five million resting CD4$^+$ lymphocytes were stimulated with latency-reversing agents (LRAs) at the indicated concentrations (20–500 nM AZ391, 100 nM JQ1, 25 μl/1x10^6 T cells αCD3/αCD28

Dynabeads (Life Technologies) for 48 hours. After LRA treatment, cells were collected, lysed and total RNA was isolated with an RNeasy kit (Qiagen). A Superscript III One-Step RT-PCR system (Life Technologies) was used to generate and pre-amplify cell-associated viral mRNA. Reaction mixes contained 15 µl of a PCR mix containing reaction mix, Superscript III, primers (900 nM final concentration) and 10 µl purified RNA. Pre-amplification was carried out using the following steps: reverse transcription at 50°C for 30 min, denaturation at 95°C for 2 min, 10 cycles of amplification (94°C 15 s, 55°C 30 s, 68°C 5 min) on a GeneAmp PCR system 9700 (Thermo Fisher). Subsequently, droplet digital PCR (ddPCR) was applied to quantify pre-amplified cDNA. Each 25 µl ddPCR mix comprised the ddPCR Probe Supermix (no dUTP), 900 nM primers, 250 nM probe, and 4 µl cDNA. The following cycling conditions were used: 10 minutes at 95°C, 40 cycles each consisting of 30 second denaturation at 94 °C followed by 59.4 °C extension for 60 seconds, and a final 10 minutes at 98°C. Reaction mixes were loaded into the Bio-Rad QX-100 emulsification device and droplets were formed following the manufacturer's instructions. Then, samples were transferred to a 96-well reaction plate and sealed with a pre-heated Eppendorf 96- well heat sealer for 2 seconds, as recommended by Bio-Rad. Finally, samples were amplified on a BioRad C1000 Thermocycler and analyzed using a BioRad QX100 ddPCR Reader.

Nucleotide coordinates are indicated relative to HXB2 consensus sequence. Primers and probe used for HIV-1 mRNA measurement were as described (Laird et al., 2015):

forward (5′→3′) CAGATGCTGCATATAAGCAGCTG (9501–9523),

reverse (5′→3′) TTTTTTTTTTTTTTTTTTTTTTTTGAAGCAC (9629–poly A),

probe (5′→3′) FAM-CCTGTACTGGGTCTCTCTGG-MGB (9531–9550).

781 Experiments where performed with $CD4^+$ T cells obtained from four individuals (1036, 2013,
782 2185, 2511). For donor 1036 average of three technical replicates is shown, for donors 2013,
783 2185 and 2511 average of the three biological replicates (±SD) is show.

784 ***T-cell activation analysis***

785 Human $CD4^+$ T cells isolated from blood (Blood Centers of the Pacific, San Francisco, CA) by
786 negative selection using RosetteSep Human $CD4^+$ T Cell Enrichment Cocktail (StemCell
787 Technologies) were incubated for 24 h in 6-well plates with AZ391 (1 μM), JQ1 (500 nM), or
788 IL-2 (20 U/ml), all dissolved in DMSO at a 1:10,000 dilution. CD69 and CD25 expression was
789 measured by flow cytometry gating on $CD3^+CD4^+$ T cells using FITC-labeled antibodies for
790 CD3 (11-0048-42, eBioscience), APC-conjugated CD25 antibodies (17-0259-42, eBioscience),
791 PerCP-labeled antibodies for CD4 (300528, Biolegend), and CD69-V450 (560740, BD Horizon).
792 Staining was performed for 30 min on ice in FACS buffer (PBS, 2% FBS), and samples were
793 analyzed on a BD Biosciences LSRII flow cytometer. Shown are the percentages of positive
794 cells relative to total CD3+CD4+ T cells or median fluorescence intensity (MFI). Data points
795 indicate four biological replicates (1-way ANOVA with Dunnett's multiple comparison test
796 $p<0.01$, $n=4$).

797 ***Ex vivo infection of tonsil-derived cells***

798 Human lymphatic aggregate culture (HLAC) cells were isolated by Ficoll-Histopaque density
799 gradient centrifugation of sheared tonsils from HIV-seronegative donors (Vanderbilt University
800 Medical Center, Nashville, TN). Isolated HLAC cells were counted, collected as pellets by
801 centrifugation at 1500 rpm for 5 min at room temperature, and re-suspended in the appropriate

volume of concentrated viral NL4.3-Luc supernatant. Typically, 50–100 ng of p24 Gag per 4×10^5 HLAC were used. Spinoculations were performed in 96-well V-bottom plates in volumes of 200 µl or less. Cells and virus were centrifuged at 2000 rpm for 1.5–2 h at room temperature. After spinoculation, cells were pooled and cultured at 1×10^6 cells/ml in RPMI 1640 containing 10% FBS and supplemented with 5 µM Saquinavir (Sigma-Aldrich) for 3 days to prevent any residual spreading infection.

For reactivation of latent HIV-1 provirus, cells were counted and collected as pellets by centrifugation at 1500 rpm for 10 min. Cells were then plated in 96-well U-bottom plates at 1×10^6 per 200 µl in the presence of 30µM Raltegravir (Santa Cruz Biotechnology) and the indicated activator. Cells were harvested 48 h after stimulation, washed one time with PBS, and lysed in 60 µl of Passive Lysis Buffer (Promega). After 15 min of lysis, the luciferase activity in cell extracts was quantified with a Perkin Elmer EnSpire 2300 Multimode plate reader after mixing 20 µl of lysate with 100 µl of substrate (Luciferase Assay System-Promega). Relative light units (RLU) were normalized to protein content determined by Bradford assay (BioRad). Data represent average (± SD) of three technical replicates per donor. Cell viability was measured with CellTiter-Blue Cell Viability Assay (Promega). Percent survival of one representative donor (#2) is shown. Data represent the average (± SD) of three technical replicates of donor #2.

In Vitro Methylation Assays

In vitro Methylation assays were performed as described (Nishioka et al., 2002). For reactions, 2 µg of histones (isolated from HEK293T cells), recombinant histone 4 (New England Biolabs), synthetic histone 4 aa 1–21 and aa 15–24 peptides (Cayman Chemical), or synthetic histone H4

aa 1–21 with a K20A mutation (GenScript) were incubated with recombinant WT SMYD2 (Sigma-Aldrich) or SMYD2 Y240F (Active Motif) in a buffer containing 50 mM Tris-HCl, pH 9, 0.01% Tween 20, 2 mM DTT and 1.1 μCi of H^3-labeled SAM (Perkin Elmer) overnight at 30°C. Reaction mixtures were fractionated on 15% SDS-PAGE for proteins or on 10–20% Tris-Tricine gradient gels for peptides (BioRad). After Coomassie staining, gels were treated with Amplify (GE Healthcare) for 30 min, dried and exposed to hyperfilm (GE Healthcare) overnight. All *in vitro* methylation assays were repeated at least three times, and representative Coomassie stain and autoradiography are shown.

Mass spectrometry analysis

Samples were denatured and reduced in 2 M urea, 10 mM NH_4HCO_3, 2 mM DTT for 30 min at 60°C, then alkylated with 2 mM iodoacetamide for 45 min at room temperature. Samples were then digested with 0.5 μg of LysC (Roche) overnight at 37C. Following digestion, samples were concentrated using C18 ZipTips (Millipore) according to the manufacturer's specifications. Desalted samples were evaporated to dryness and resuspended in 0.1% formic acid for mass spectrometry analysis.

Digested samples were analyzed in technical duplicate on a Thermo Fisher Orbitrap Fusion mass spectrometry system equipped with an Easy nLC 1200 ultra-high pressure liquid chromatography system interfaced via a Nanospray Flex nanoelectrospray source. Samples were injected on a C18 reverse phase column (25 cm x 75 um packed with ReprosilPur C18 AQ 1.9 um particles). Peptides were separated by an organic gradient from 5–30% ACN in 0.1% formic acid over 112 minutes at a flow rate of 300 nl/min. The MS continuously acquired spectra in a data-dependent manner throughout the gradient, acquiring a full scan in the Orbitrap (at 120,000

resolution with an AGC target of 200,000 and a maximum injection time of 100 ms) followed by as many MS/MS scans as could be acquired on the most abundant ions in 3s in the dual linear ion trap (rapid scan type with an intensity threshold of 5000, HCD collision energy of 29%, AGC target of 10,000, a maximum injection time of 35 ms, and an isolation width of 1.6 m/z). Singly and unassigned charge states were rejected. Dynamic exclusion was enabled with a repeat count of 1, an exclusion duration of 20 s, and an exclusion mass width of +/- 10 ppm.

Raw mass spectrometry data were assigned to histone H4 sequences with the MaxQuant software package (version 1.5.5.1) (Cox and Mann, 2008). Variable modifications were allowed for N-terminal protein acetylation, methionine oxidation, and lysine methylation. A static modification was indicated for carbamidomethyl cysteine. All other settings were left as MaxQuant defaults. MaxQuant-identified peptides were quantified by MS1 filtering using the Skyline software suite (Maclean et al., 2010).

Quantification and Statistical Analysis

All values are depicted as mean ± SD. Statistical parameters including statistical analysis, statistical significance, and n value are reported in the Figure legends and Supplementary Figure legends. Statistical analyses were performed using Prism Software (GraphPad). For statistical comparison of ChIP experiments, standard t-test was used. A value of $p < 0.05$ was considered significant. For statistical analysis of T-cell activation experiments 1-way ANOVA with Dunnett's multiple comparison test $p<0.01$, $n=4$ was employed.

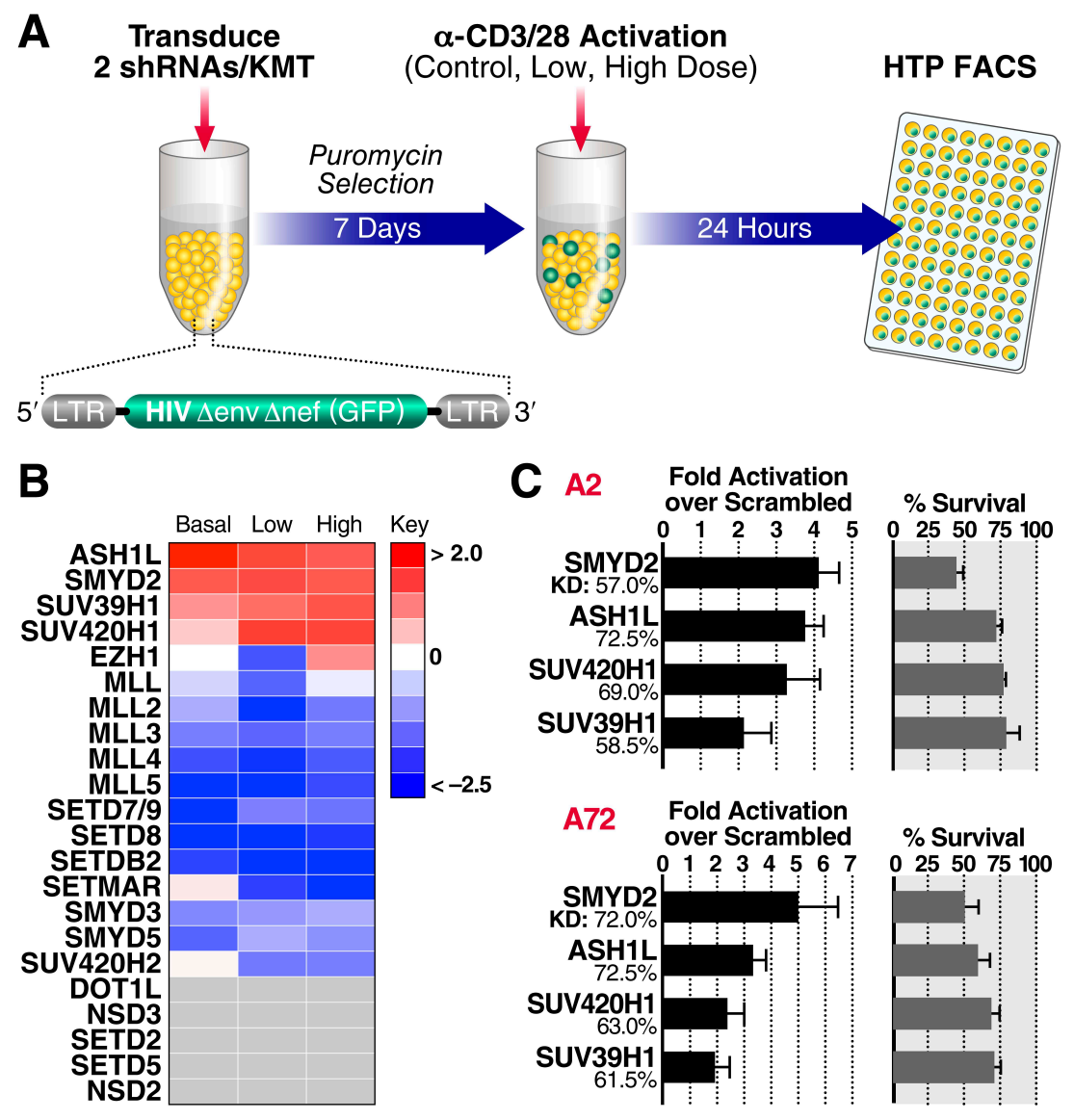
A
Transduce
2 shRNAs/KMT
α-CD3/28 Activation
(Control, Low, High Dose)
HTP FACS
Puromycin
Selection
7 Days
24 Hours
5′ LTR HIV Δenv Δnef (GFP) LTR 3′
B
Basal Low High Key
> 2.0
0
< –2.5
ASH1L
SMYD2
SUV39H1
SUV420H1
EZH1
MLL
MLL2
MLL3
MLL4
MLL5
SETD7/9
SETD8
SETDB2
SETMAR
SMYD3
SMYD5
SUV420H2
DOT1L
NSD3
SETD2
SETD5
NSD2
C
A2
Fold Activation over Scrambled
0 1 2 3 4 5
% Survival
0 25 50 75 100
SMYD2 KD: 57.0%
ASH1L 72.5%
SUV420H1 69.0%
SUV39H1 58.5%
A72
Fold Activation over Scrambled
0 1 2 3 4 5 6 7
% Survival
0 25 50 75 100
SMYD2 KD: 72.0%
ASH1L 72.5%
SUV420H1 63.0%
SUV39H1 61.5%

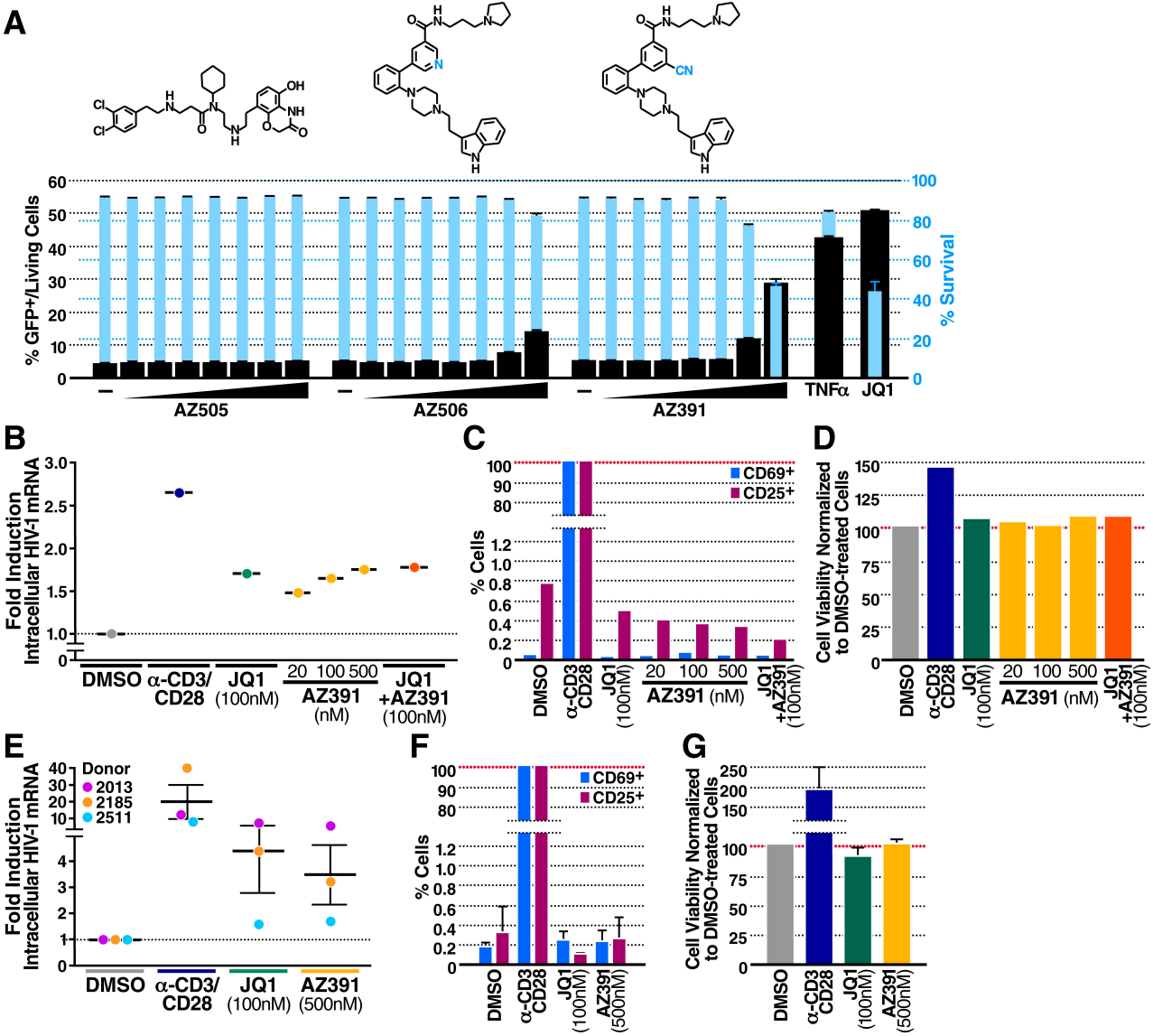
A
% GFP+/Living Cells
% Survival
AZ505
AZ506
AZ391
TNFα
JQ1
B
Fold Induction Intracellular HIV-1 mRNA
DMSO
α-CD3/ CD28
JQ1 (100nM)
AZ391 (nM)
JQ1 +AZ391 (100nM)
C
% Cells
CD69+
CD25+
D
Cell Viability Normalized to DMSO-treated Cells
E
Donor
2013
2185
2511
AZ391 (500nM)
F
G

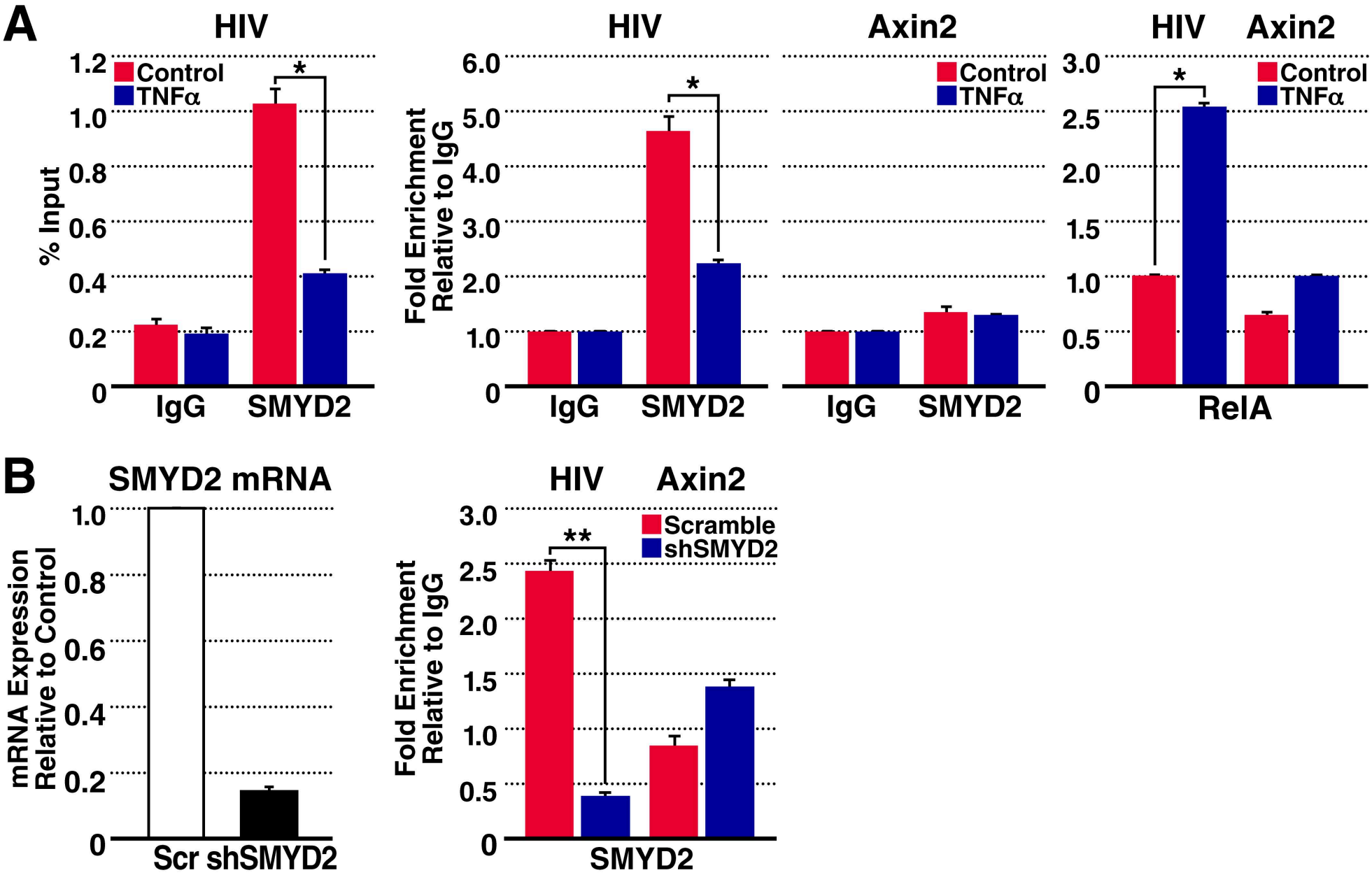
A
HIV
% Input
1.2
1.0
0.8
0.6
0.4
0.2
0
Control
TNFα
*
IgG
SMYD2
HIV
Fold Enrichment Relative to IgG
6.0
5.0
4.0
3.0
2.0
1.0
0
*
IgG
SMYD2
Axin2
Control
TNFα
IgG
SMYD2
HIV
Axin2
3.0
2.5
2.0
1.5
1.0
0.5
0
*
Control
TNFα
RelA
B
SMYD2 mRNA
mRNA Expression Relative to Control
1.0
0.8
0.6
0.4
0.2
0
Scr
shSMYD2
HIV
Axin2
Fold Enrichment Relative to IgG
3.0
2.5
2.0
1.5
1.0
0.5
0
**
Scramble
shSMYD2
SMYD2

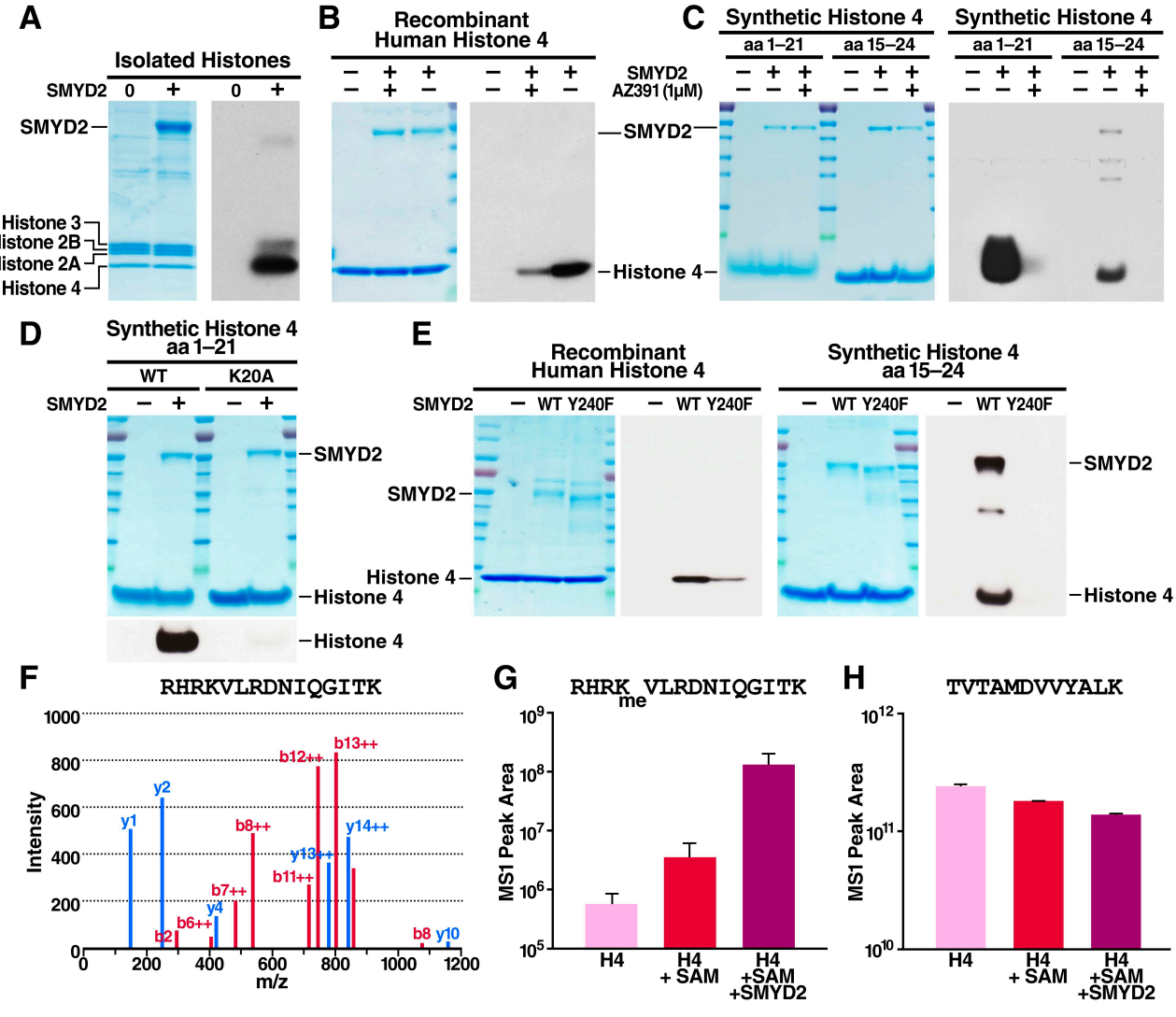
A
Isolated Histones
SMYD2 0 + 0 +
SMYD2
Histone 3
Histone 2B
Histone 2A
Histone 4
B
Recombinant Human Histone 4
SMYD2
Histone 4
C
Synthetic Histone 4
aa 1–21
aa 15–24
SMYD2
AZ391 (1μM)
SMYD2
Histone 4
D
Synthetic Histone 4 aa 1–21
WT
K20A
SMYD2
SMYD2
Histone 4
Histone 4
E
Recombinant Human Histone 4
Synthetic Histone 4 aa 15–24
SMYD2
WT Y240F
SMYD2
Histone 4
SMYD2
Histone 4
F
RHRKVLRDNIQGITK
Intensity
m/z
y1
y2
b2
b6++
y4
b7++
b8++
b11++
b12++
y13++
b13++
y14++
b8
y10
G
RHRK me VLRDNIQGITK
MS1 Peak Area
H4
H4 + SAM
H4 +SAM +SMYD2
H
TVTAMDVVYALK
MS1 Peak Area
H4
H4 + SAM
H4 +SAM +SMYD2

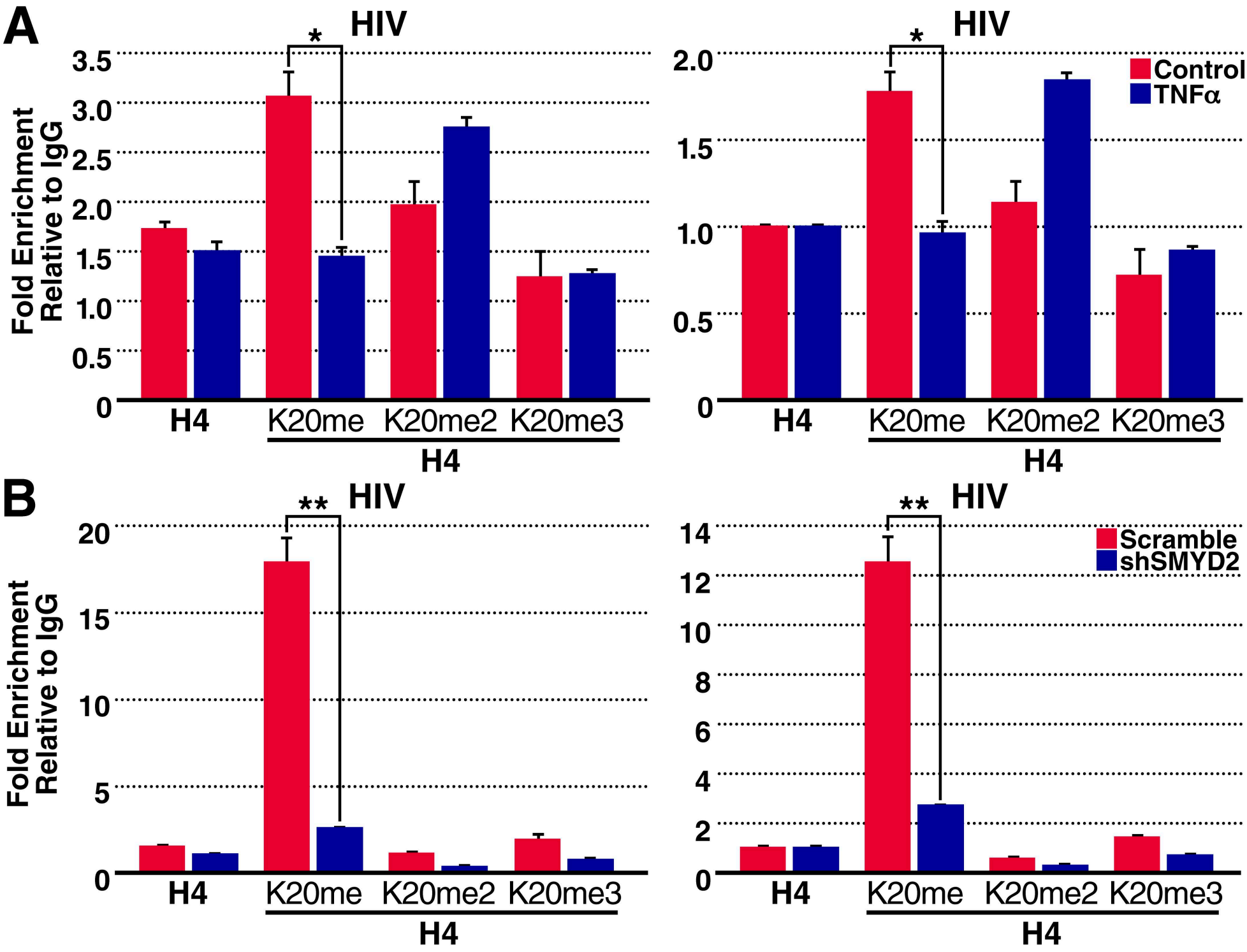
A
HIV
*
Fold Enrichment Relative to IgG
3.5
3.0
2.5
2.0
1.5
1.0
0.5
0
H4
K20me
K20me2
K20me3
H4
HIV
*
Control
TNFα
2.0
1.5
1.0
0.5
0
H4
K20me
K20me2
K20me3
H4
B
HIV
**
Fold Enrichment Relative to IgG
20
15
10
5
0
H4
K20me
K20me2
K20me3
H4
HIV
**
Scramble
shSMYD2
14
12
10
8
6
4
2
0
H4
K20me
K20me2
K20me3
H4

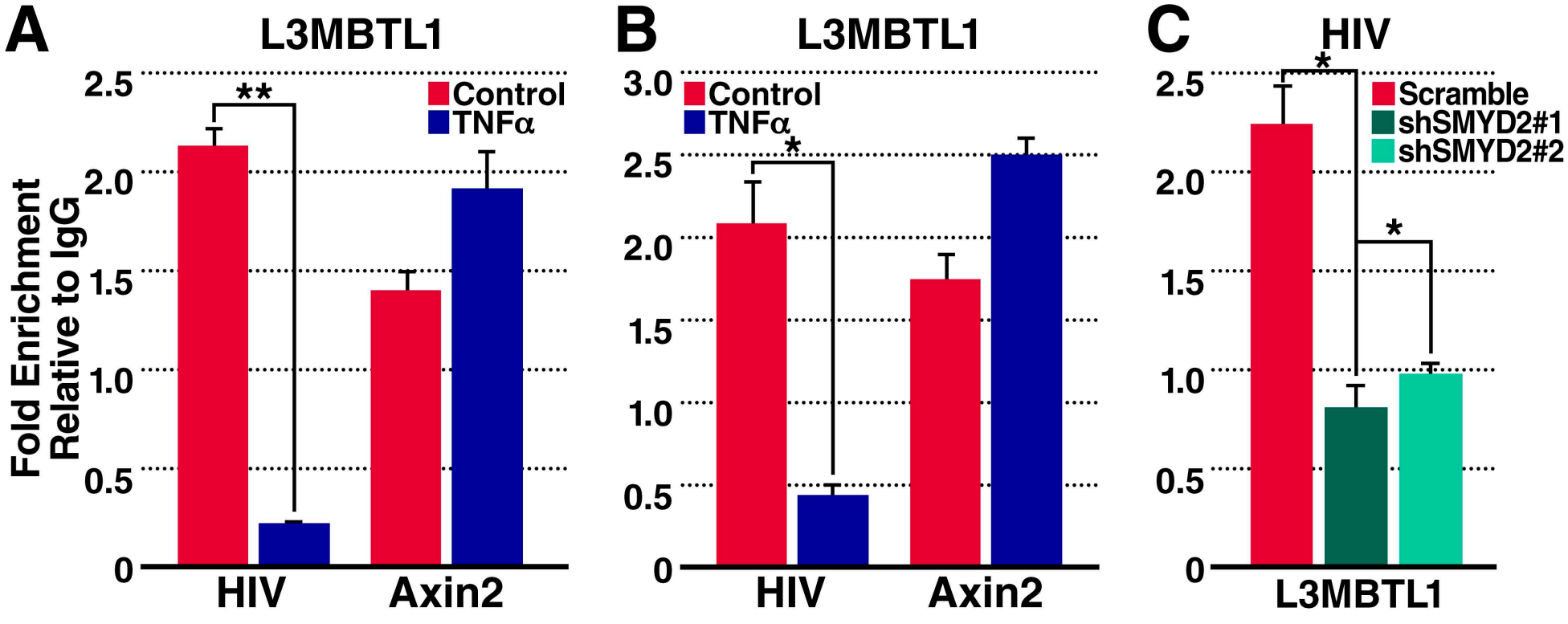
A
L3MBTL1
Fold Enrichment Relative to IgG
2.5
2.0
1.5
1.0
0.5
0
**
Control
TNFα
HIV
Axin2
B
L3MBTL1
3.0
2.5
2.0
1.5
1.0
0.5
0
*
Control
TNFα
HIV
Axin2
C
HIV
2.5
2.0
1.5
1.0
0.5
0
*
*
Scramble
shSMYD2#1
shSMYD2#2
L3MBTL1

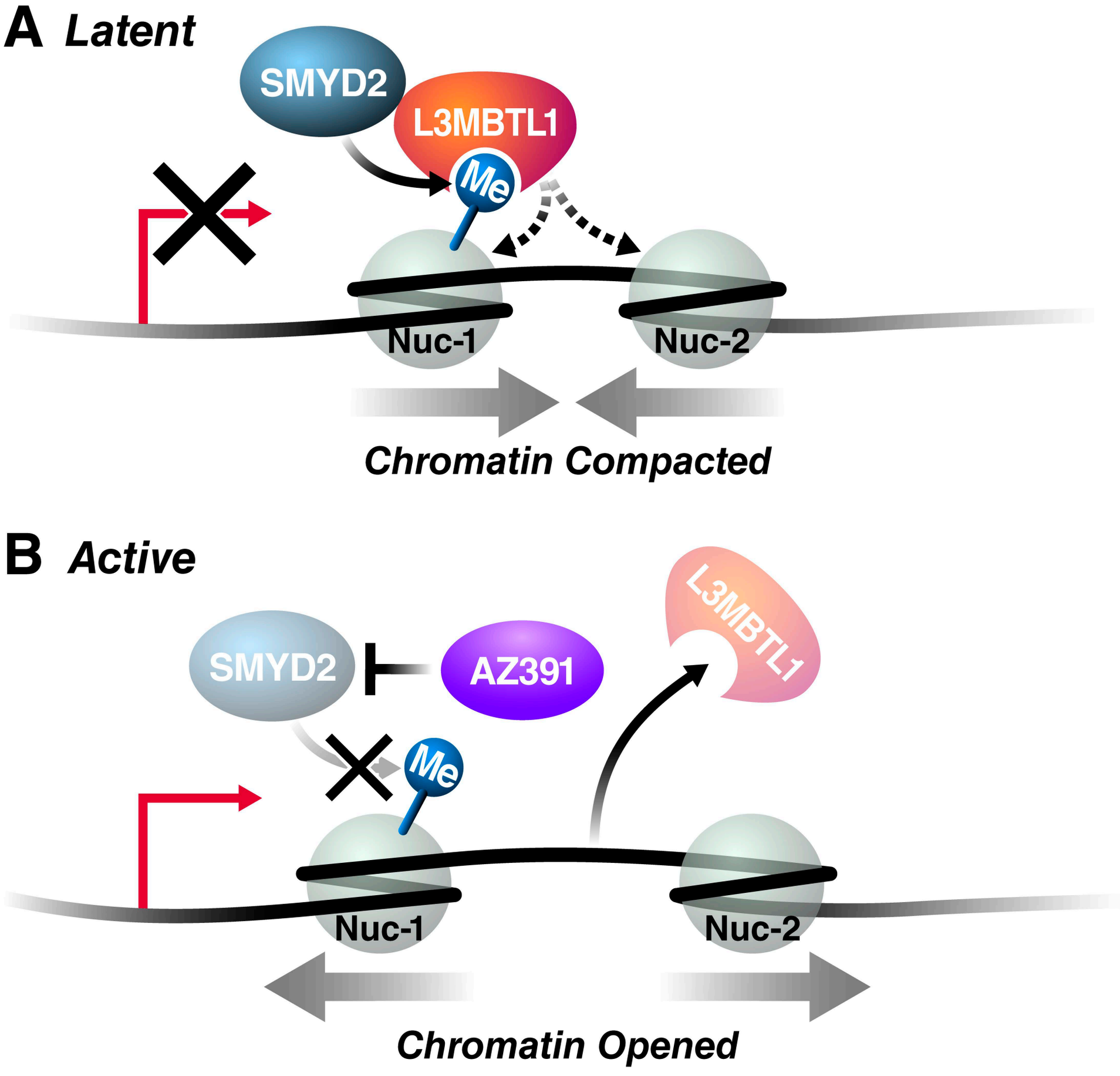
A Latent
SMYD2
L3MBTL1
Me
Nuc-1
Nuc-2
Chromatin Compacted
B Active
SMYD2
AZ391
L3MBTL1
Me
Nuc-1
Nuc-2
Chromatin Opened

Supplemental Information

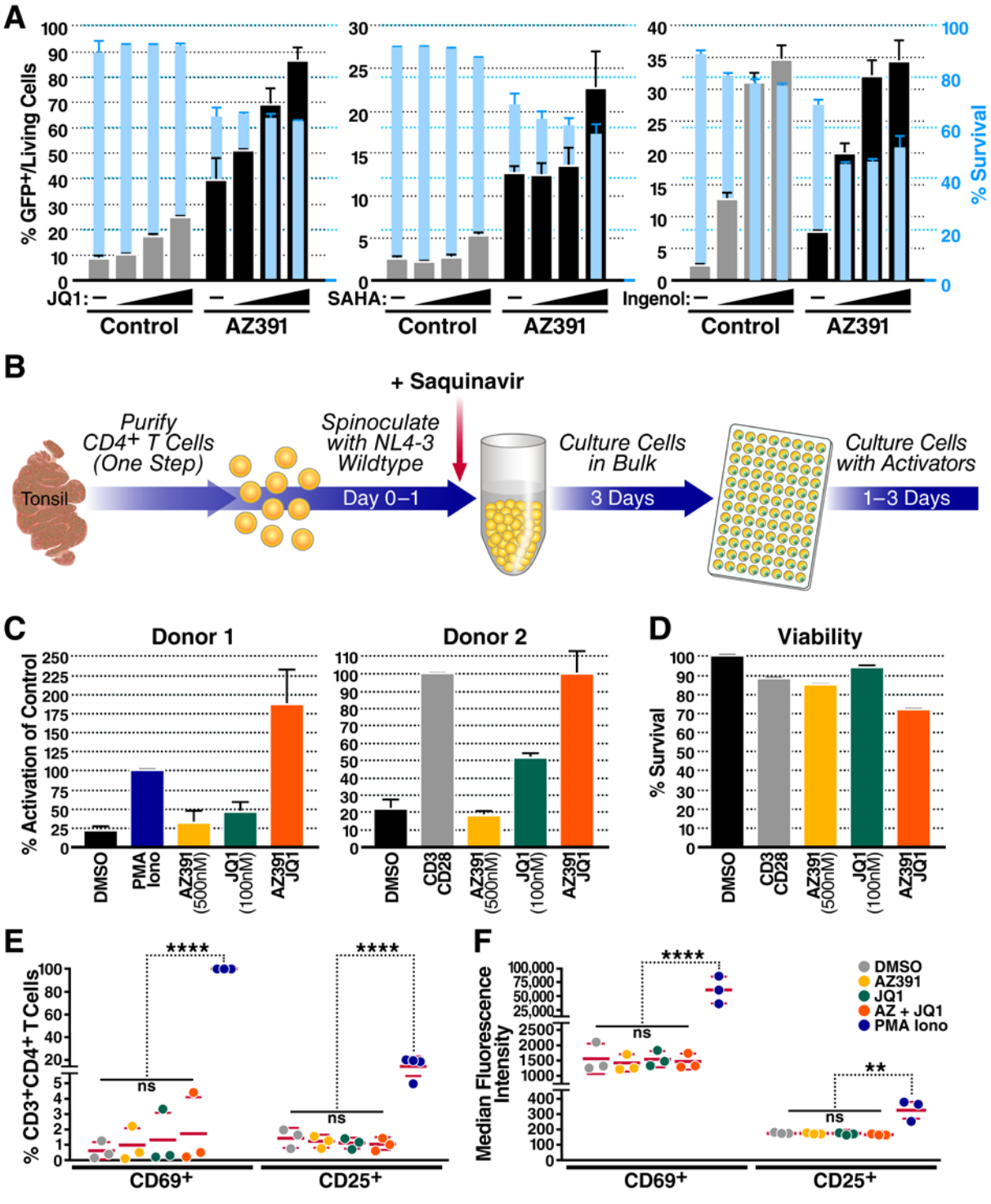

Supplemental Figure 1: Reactivation of latent HIV-1 with SMYD2 inhibitor AZ391. (a) J-Lat cell line A72 was treated with SMYD2 inhibitor AZ391 at increasing concentrations (10 nM–5 µM) combined with increasing amounts of other LRAs (JQ1; SAHA, an HDAC inhibitor; ingenol dibenzoate, a protein kinase C agonist) for 18 h and analyzed by flow cytometry. More than additive effects with JQ1, less with SAHA, and practically no combination effect with ingenol 3,20-dibenzoate and AZ391 was observed. Data represent average (± SD) of three independent experiments. **(b)** Scheme of the primary HLAC latency model. **(c)** A combination of PMA/Ionomycin (blue) or αCD3/αCD28 (grey) was used to induce maximal reactivation. Results are expressed as percentage of reactivation relative to values obtained in control-induced cells in each donor. In two donors, addition of AZ391 (yellow), JQ1 (green) or a combination of both were tested in addition to PMA/Ionomycin or αCD3/αCD28 (grey). Data represent average (± SD) of three technical replicates per donor. **(d)** Cell viability was measured with CellTiter-Blue Cell Viability Assay (Promega). Percent survival of one representative donor (#2) is shown. Data represent the average (± SD) of three technical replicates of donor #2. **(e–f)** Flow cytometry of T-cell activation marker CD25 and CD69 in human $CD4^+$ T-cells isolated from blood and incubated with AZ391 (1 µM) and/or JQ1 (500 nM), or PMA (10 ng/ml) and Ionomycin (500 nM). Shown are the percentages of positive cells relative to total $CD3^+CD4^+$ T cells **(e)** or median fluorescence intensity (MFI) **(f).** Data points indicate four biological replicates (1-way ANOVA with Dunnett's multiple comparison test $p<0.01$, $n=4$).

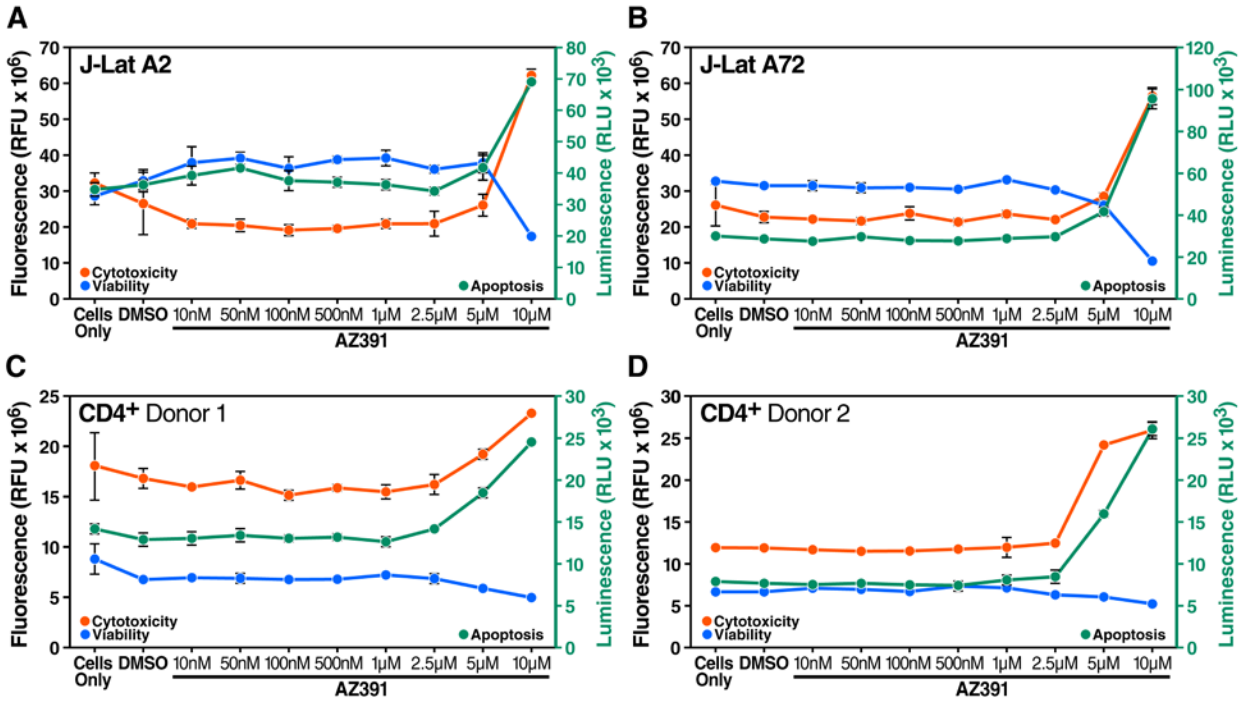

Supplemental Figure 2: Measurement of Viability, Cytotoxicity and Apoptosis of AZ391 treated cells. ApoTox-Glo^{TM} Triplex Assays (Promega) were performed in AZ391-treated A2 J-Lat cells **(a)**, A72 J-Lat cells **(b)**, and primary CD4^{+} T cells from 2 independent blood donors **(c)**. AZ391 treatment did not reduce viability nor increase cytotoxicity and caspase-3/7 activity at concentrations lower than 5 µM. All measurements were repeated at least three times and average of one experiment of three technical replicates (±SD) are shown.

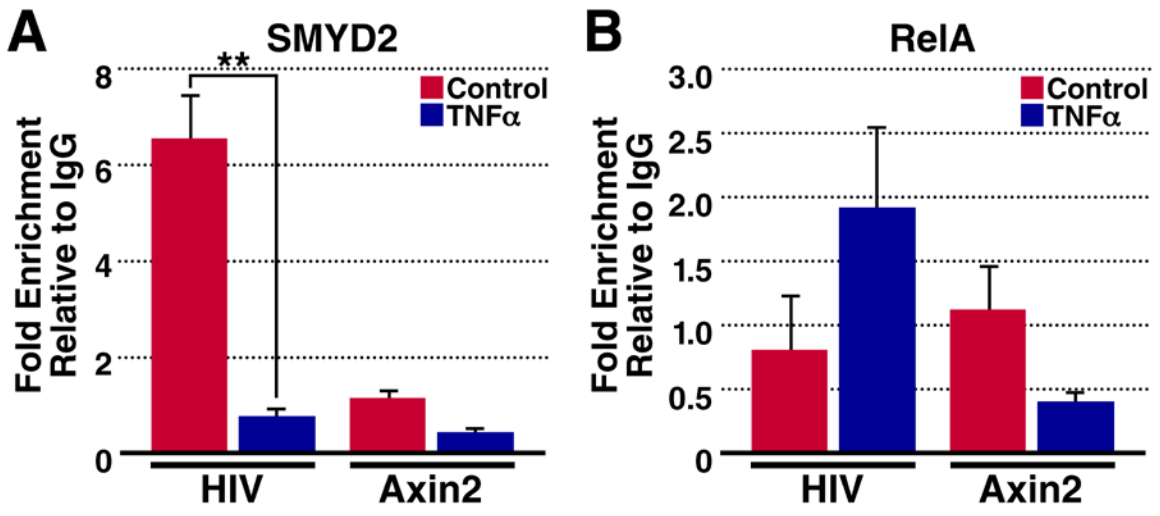

Supplemental Figure 3: SMYD2 associates with the HIV promoter in cells. (a) ChIP experiments of SMYD2 in A2 J-Lat cells, either non-stimulated (red) or in response to TNFα stimulation (blue) at the HIV LTR nuc-1 region (left) or at the Axin2 gene (right). SMYD2 is present at the HIV-LTR under non-stimulated conditions (red) and was displaced in response to TNFα stimulation (blue) at the HIV LTR. All ChIPs and qPCRs were repeated at least three times, and representative results of three technical replicates are shown. **(b)** ChIP experiments of RelA in A2 J-Lat cells, either non-stimulated (red) or in response to TNFα stimulation (blue) at the HIV LTR nuc-1 region (left) or at the Axin2 gene (right). RelA is recruited to the HIV promoter after treatment with TNFα (blue). No association of SMYD2 or RelA with Axin2 was observed. All ChIPs and qPCRs were repeated at least three times, and representative results of three technical replicates are shown. For statistical comparison of ChIP experiments, the difference in dis-enrichment between control and TNFα treatment was calculated and 3 biological replicates were analyzed by t-test. A value of $p < 0.05$ was considered significant.

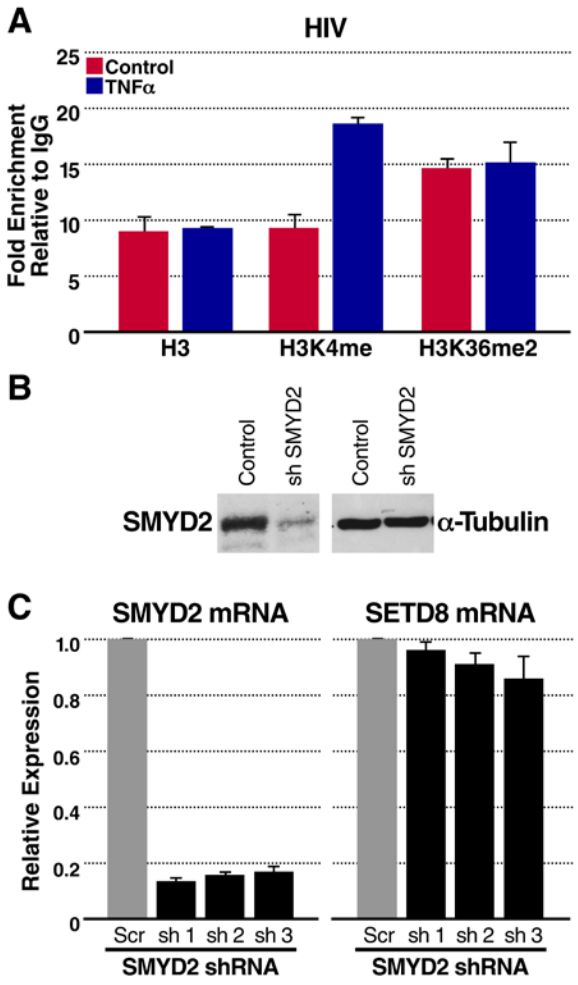

Supplemental Figure 4: (a) ChIP experiments of histone 3 lysine 4 (H3K4me1) and histone 3 lysine 36 (H3K36me2) in A2 J-Lat cell lines, either non-stimulated (red) or in response to TNFα stimulation (blue) at the HIV LTR nuc-1 region (left) or at the Axin2 gene (right). H3K36me2 remained unchanged in control and activated cells, while H3K4me1 was enriched ~ twofold in response to TNFα. Results are shown relative to IgG control. All ChIPs and qPCRs were repeated at least three times, and representative results of three technical replicates are shown. **(b)** SMYD2 knockdown was confirmed by western blotting in A72 J-Lat cells. **(C)** RNA was isolated from A72 J-Lat cells and mRNA levels were analyzed by RT-qPCR and normalized to RPL13A RNA. SMYD2 knockdown did not change expression level of SETD8.

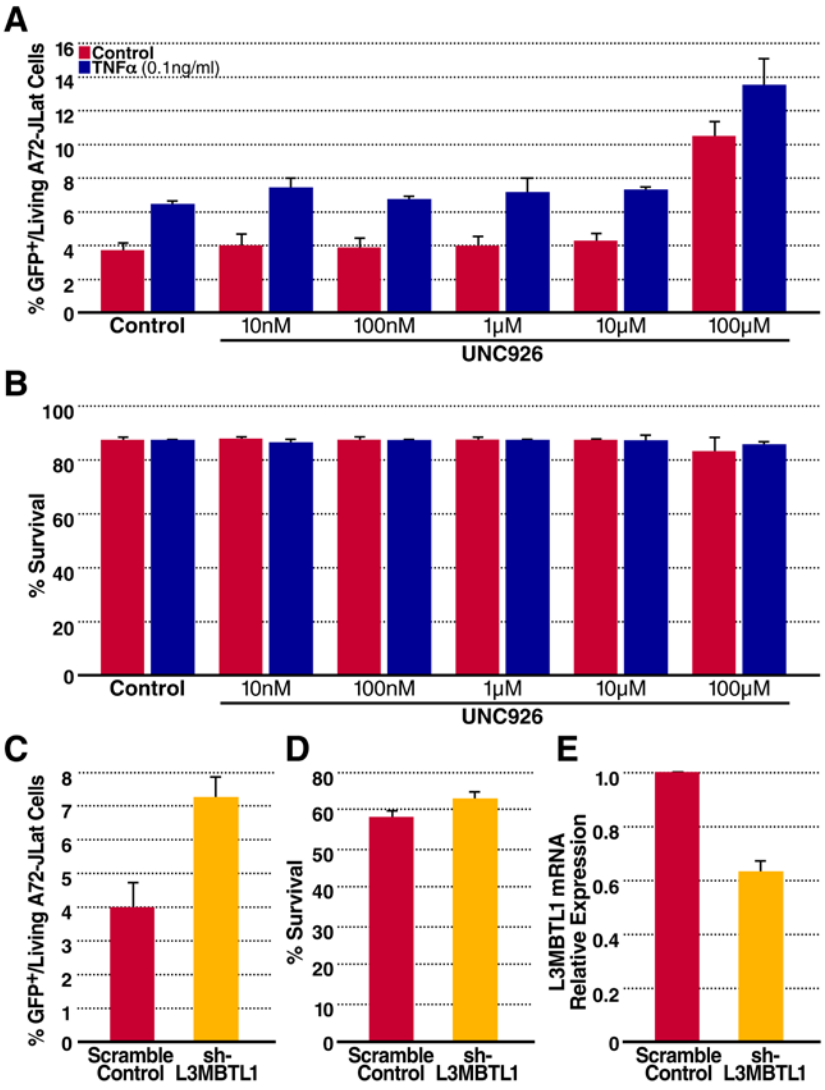

Supplemental Figure 5: (a) Reactivation of latent HIV-1 with L3MBTL1 inhibitor UNC926 or shRNA mediated knockdown of L3MBTL1. (a/b) J-Lat cell line A72 was treated with L3MBTL1 inhibitor UNC926 (K_d = 3.9 μM) at increasing concentrations (10 nM–100 μM) without or combined with 0.1 ng/ml TNFα for 18 h and analyzed by flow cytometry. Activation is observed only at 100 μM given the low affinity of UNC926 **(a).** No effect on viability as measured by forward-side scatter analysis is observed even at high drug concentrations **(b)**. Data represent average (± SD) of three independent experiments. **(c)** Percentage of GFP^+ A72 J-Lat

cells after shRNA-mediated L3MBTL1 knockdown. Data represent average (± SD) of three independent experiments. **(d)** Cell viability was monitored by forward-side scatter analysis. **(e)** ShRNA knockdown was confirmed using qPCR and did not exceed ~40% knockdown.

Supplemental Table 1: Small hairpin RNA (shRNA) screen of 31 cellular KMTs in the $CD4^+$ J-Lat 5A8 cell line harboring a latent full-length HIV provirus with the fluorescent marker GFP inserted into the *nef* open-reading frame to allow monitoring of transcriptional activity by flow cytometry.

Gene	Plate#	TRC#	Batch 1	Batch 1	Batch 1	Batch 2	Batch 2	Batch 2	Average 1/2	Ave. 1/2	Ave. 1/2
			No ab	0.125µg	1µg	No ab	0.125µg	1µg	No Ab	0.125	1µg
NF-κB RelA		TRCN0000353629	-2.152	-1.755		-2.567	-1.981	-2.133			
EZH2	1D9	TRCN0000040074	-1.387	-1.020		-1.045	1.239	1.168			
EZH2	1D10	TRCN0000040075	1.265	1.178		-1.012	1.051	-1.066			
SETD7	1E1	TRCN0000078628	-1.742	-1.113		-1.610	-1.059	-1.203			
SETD7	1E2	TRCN0000078631	-1.283	-1.234		-1.752	-1.476	-1.615			
EHMT2	1E4	TRCN0000115667	-2.502	-1.073		-1.706	1.010	-1.106			
EHMT2	1E5	TRCN0000115668	-1.270	1.012		-1.786	1.051	-1.090			
DOT1L	2B2	TRCN0000236345	3.130	1.302		5.704	2.057	1.736			
DOT1L	2B3	TRCN0000236343	-1.452	-1.844		-4.066	-1.754	-1.950			
SETD1B	2B6	TRCN0000237962	-1.732	-1.178		-3.609	-1.139	-1.252			
SETD1B	2B7	TRCN0000237964	1.294	-1.340		-1.764	-1.241	-1.444			
NSD1	2C3	TRCN0000238373	-1.695	-1.288		-2.058	-1.086	-1.231			
NSD1	2C4	TRCN0000238372	1.486	1.098		1.029	1.220	1.102			
NF-κB RelA		TRCN0000353629	-1.883	-2.512	-2.335	-1.709	-2.137	-2.109	-1.796	-2.325	-2.222
ASH1	2C8	TRCN0000246167	-1.171	-1.005	1.098	-1.058	-1.281	-1.242	-1.115	-1.143	-0.072
ASH1	2C9	TRCN0000246168	1.467	1.582	1.320	1.194	1.673	1.611	1.330	1.627	1.466
MLL	1A5	TRCN0000005954	-1.310	-1.824	1.006	-1.478	-1.785	-1.474	-1.394	-1.805	-0.234
MLL	1A6	TRCN0000005956	-2.635	-1.294	1.108	-2.278	1.068	1.309	-2.457	-0.113	1.209
SUV39H1	1F5	TRCN0000158337	-1.192	1.259	1.529	-1.404	1.389	1.501	-1.298	1.324	1.515
SUV39H1	1F6	TRCN0000157251	-2.683	1.366	1.408	-1.748	-1.376	-1.111	-2.215	-0.005	0.149
SUV39H2	1B2	TRCN0000006938	-2.097	-1.250	-1.005	-1.704	-1.588	-1.186	-1.901	-1.419	-1.095
SUV39H2	3C4	TRCN0000011057	-1.834	-1.351	-1.153	-1.701	-1.374	-1.098	-1.768	-1.362	-1.126
SUV420H1	2F8	TRCN0000359162	-1.375	-1.107	-1.022	1.004	-1.203	-1.146	-0.185	-1.155	-1.084
SUV420H1	2F9	TRCN0000359230	1.447	1.590	1.596	1.942	1.830	1.698	1.695	1.710	1.647
SUV420H2	2F10	TRCN0000145137	1.341	-3.269	-2.342	-1.219	-1.460	-1.145	0.061	-2.365	-1.743
SUV420H2	2F11	TRCN0000143270	-1.636	-1.780	-1.393	1.007	-1.708	-1.461	-0.314	-1.744	-1.427
MLL2	1B7	TRCN0000013138	-3.660	-2.054	-1.388	-3.227	-2.416	-1.637	-3.444	-2.235	-1.513
MLL2	1B8	TRCN0000013140	-2.313	-2.134	-1.257	-2.345	-2.161	-1.296	-2.329	-2.148	-1.277
MLL3	1B3	TRCN0000008742	-2.683	-1.692	-1.511	-2.813	-1.807	-1.547	-2.748	-1.749	-1.529
MLL3	1B4	TRCN0000008743	-1.574	-1.816	-1.384	-2.673	-1.675	-1.257	-2.123	-1.745	-1.321
MLL4	1A8	TRCN0000005958	-4.466	-2.338	-1.610	-3.879	-2.480	-2.139	-4.172	-2.409	-1.875
MLL4	1A9	TRCN0000005959	-1.170	-1.022	1.087	-1.731	-1.567	-1.121	-1.450	-1.295	-0.017
NF-κB RelA		TRCN0000353629	-2.830	-2.605	-2.397	-1.344	-2.216	-2.193	-2.087	-2.410	-2.295
NSD2	A6	TRCN0000019816	-2.406	-2.843	-1.913	-1.183	-2.969	-2.301	-1.795	-2.906	-2.107
NSD2	H5	TRCN0000019817	1.274	1.455	1.338	1.389	1.483	1.524	1.331	1.469	1.431
MLL5	1F3	TRCN0000150550	-7.679	-3.184	-2.185	-2.012	-2.841	-1.999	-4.846	-3.012	-2.092
MLL5	1F4	TRCN0000154711	-2.941	-1.324	-1.197	-1.087	-1.047	1.120	-2.014	-1.185	-0.039
EHMT1	1D7	TRCN0000036054	-3.261	-1.162	-1.047	-1.148	1.098	1.252	-2.204	-0.032	0.103
EHMT1	1D8	TRCN0000036057	1.406	-1.121	-1.104	1.052	1.008	1.024	1.229	-0.056	-0.040
SETD8	1E9	TRCN0000148268	-4.731	-3.410	-2.615	-2.169	-2.830	-1.883	-3.450	-3.120	-2.249
SETD8	1E10	TRCN0000130036	-2.942	-2.284	-1.768	-1.771	-1.810	-1.414	-2.356	-2.047	-1.591

NF-κB RelA		TRCN0000353629	-1.374	-2.530	-2.339	-1.234	-1.594	-1.727	-1.304	-2.062	-2.033
SETDB1	1G1	TRCN0000147130	-1.018	1.208	1.359	1.096	1.014	1.034	0.039	1.111	1.197
SETDB1	1G2	TRCN0000179094	3.306	1.370	1.380	2.630	1.233	1.131	2.968	1.301	1.256
SETDB2	1F7	TRCN0000159172	-2.379	-2.934	-2.478	-1.931	-2.790	-2.728	-2.155	-2.862	-2.603
SETDB2	1F8	TRCN0000160242	1.078	-2.433	-2.625	1.352	-2.295	-2.018	1.215	-2.364	-2.321
SETMAR	1G7	TRCN0000146300	1.672	-2.471	-2.703	-1.234	-1.876	-2.274	0.219	-2.174	-2.488
SETMAR	1G8	TRCN0000179441	-1.328	-1.259	-1.014	1.144	-1.206	-1.385	-0.092	-1.233	-1.199
SETD5	2D11	TRCN0000253861	1.685	1.420	1.414	1.300	1.455	1.253	1.493	1.437	1.333
SETD5	1D12	TRCN0000253863	1.064	-1.876	-1.476	1.053	-1.822	-1.503	1.059	-1.849	-1.489
NF-κB RelA		TRCN0000353629	-1.652	-2.757	-2.277	-1.374	-2.203	-2.333	-1.513	-2.480	-2.305
SETD2	1A3	TRCN0000003030	-1.987	1.978	1.968	-2.134	1.560	1.502	-2.060	1.769	1.735
SETD2	1A4	TRCN0000003032	-1.303	-2.912	-1.911	-1.347	-2.284	-1.823	-1.325	-2.598	-1.867
EZH1	3B1	TRCN0000355734	-1.678	-2.254	1.013	-1.654	-1.629	1.059	-1.666	-1.941	1.036
EZH1	3B2	TRCN0000355735	-1.415	1.014	1.328	-1.221	1.202	1.151	-1.318	1.108	1.239
SETD6	3B4	TRCN0000419700	1.096	-1.506	-1.258	-1.179	-1.112	1.216	-0.041	-1.309	-0.021
SETD6	3B5	TRCN0000417114	-1.340	-1.152	1.060	-1.852	1.043	1.030	-1.596	-0.054	1.045
DOT1L	2B2	TRCN0000236345	4.712	1.837	1.517	6.883	2.316	1.749	5.797	2.076	1.633
DOT1L	2B3	TRCN0000236343	-3.947	-2.420	-1.918	-3.456	-2.173	-1.798	-3.702	-2.297	-1.858
MLL2	1B7	TRCN0000013138	-3.022	-2.572	-1.617	-3.432	-2.397	-1.457	-3.227	-2.485	-1.537
MLL2	1B8	TRCN0000013140	-1.459	-2.360	-1.812	-2.005	-2.381	-1.679	-1.732	-2.371	-1.746
NF-κB RelA		TRCN0000353629	-2.567	-2.693	-2.284	-1.091	-2.386	-2.638	-1.829	-2.540	-2.461
DOT1L	2B4	TRCN0000236342	-1.573	-1.453	-1.429	-1.314	-2.021	-1.455	-1.444	-1.737	-1.442
DOT1L	2B5	TRCN0000236344	-3.878	1.246	1.487	-3.795	-1.234	1.171	-3.837	0.006	1.329
MLL2	2A10	TRCN0000235742	-2.811	-1.012	1.440	-1.599	-1.260	1.068	-2.205	-1.136	1.254
MLL2	2A11	TRCN0000235743	-2.403	1.024	1.371	-2.046	-1.207	1.017	-2.224	-0.092	1.194
SUV420H2	1F10	TRCN0000145137	-3.046	1.317	1.184	-1.295	-1.273	-1.299	-2.171	0.022	-0.058
SUV420H2	1F11	TRCN0000143270	1.217	-1.701	-1.638	-1.034	-1.387	-1.367	0.092	-1.544	-1.502
SUV420H2	3C1	TRCN0000437411	-2.171	1.300	1.329	-1.719	-1.035	1.048	-1.945	0.132	1.188
SUV420H2	3C2	TRCN0000446372	1.586	1.328	1.133	1.402	1.226	1.072	1.494	1.277	1.103

Supplemental Table 2: Characteristics of HIV-1–infected study participants. Four HIV-1-infected individuals, who met the criteria of suppressive ART, which is undetectable plasma HIV-1 RNA levels (<50 copies/ml) for a minimum of six months, and a $CD4^+$ T cell count of at least 350 cells/mm^3, were enrolled. The participants were recruited from the SCOPE cohorts at the University of California, San Francisco.

Patient ID	**Age**	**Gender**	**Ethnicity**	**CD4 T cell count**	**Year of first HIV+ test**	**ART Regimen**	**Peak self-reported VL (copies ml-1)**
#2013	68	Male	White	715	1986	ABC/TCV/3TC	110000
#2511	48	Male	White	334	2001	EFV/TDF/FTC,RGV	489873
#2158	60	Male	African American	434	1999	TMQ	128447
#1036	48	Male	African American	410	1990	EGV/TDF/FTC/COBI	132724

ABC, abacavir; TCV, tivicay; 3TC, lamivudine; EFV, Efavirenz; TDF, tenofovir; FTC, emtricitabine; RGV, raltegravir; TMQ, Triumeq; EGV, Elvitegravir; COBI, Cobicistat.

Supplemental Table 3: TRC numbers and Target sequence of shRNA clones used in the manuscript.

Gene	TRC Number	Target Sequence
ASH1L	TRCN0000246167	GAGTCGATTGATCCAATTAAA
ASH1L	TRCN0000246168	CGTCTACGAAAGGCCTATTAC
DOT1L	TRCN0000236345	TCGCCAACACGAGTGTTATAT
DOT1L	TRCN0000236343	CACGTTGAACAAGTGCATTTA
DOT1L	TRCN0000236342	CACATTGGAGAGAGGCGATTT
DOT1L	TRCN0000236344	GCCCGCAAGAAGAAGCTAAAC
EHMT1	TRCN0000036054	CGAGTCAATAACGCCAGCTAT
EHMT1	TRCN0000036057	CCTCGGTTCTGAGTCGTATAA
EHMT2	TRCN0000115667	CACACATTCCTGACCAGAGAT
EHMT2	TRCN0000115668	CCTCTTCGACTTAGACAACAA
EZH1	TRCN0000355734	AGACGTGCAAGCAGGTCTTTC
EZH1	TRCN0000355735	CTATCTGGCAGTGCGAGAATG
EZH2	TRCN0000040074	GCTAGGTTAATTGGGACCAAA
EZH2	TRCN0000040075	CCAACACAAGTCATCCCATTA
MLL	TRCN0000005954	GCACTGTTAAACATTCCACTT
MLL	TRCN0000005956	CGCCTAAAGCAGCTCTCATTT
MLL2	TRCN0000235742	CATCTACATGTTCCGAATAAA
MLL2	TRCN0000235743	CGTAGAAGAGGACCTACTAAT
MLL2	TRCN0000013138	CCCACCTGAATCATCACCTTT
MLL2	TRCN0000013140	CCTCGCCTCAAGAAATGGAAA
MLL3	TRCN0000008742	GAGGCGATTCAACACACCATT
MLL3	TRCN0000008743	CCCTGTTAGAATGCCCAGTTT
MLL4	TRCN0000005958	ACCCTCATGTTCAGGGTGGAT
MLL4	TRCN0000005959	CCAGCACTATAAGTTCCGTTA
MLL5	TRCN0000150550	GCTGATTTGATGCTGTATGAT
MLL5	TRCN0000154711	GCTGTTCCCTTCCAGATTTAA
NSD1	TRCN0000238373	GTGCTAATTTCACGGTATAAA
NSD1	TRCN0000238372	CCGAGACGTCTCAGGTTAATC
NSD2	TRCN0000019816	CCTCTCTTTGAATCTTCCATT
NSD2	TRCN0000019817	CGGAAAGCCAAGTTCACCTTT
SETD1B	TRCN0000237962	GGAGATTACCTATGACTATAA
SETD1B	TRCN0000237964	ACATGCGGGAGAAGCGTTATG
SETD2	TRCN0000003030	CCTGAAGAATGATGAGATAAT
SETD2	TRCN0000003032	GCCCTATGACTCTCTTGGTTA
SETD5	TRCN0000253861	AGCGTGTATTCCACTCATAAT
SETD5	TRCN0000253863	AGACTTGTTGAGCCCATTAAA
SETD6	TRCN0000419700	GACCTATGCCACAGACTTAAA
SETD6	TRCN0000417114	GTGGACATACGGTAGTAATAA
SETD7/9	TRCN0000078628	GCCAGGGTATTATTATAGAAT
SETD7/9	TRCN0000078631	CTTATGAATCAGAAAGGGTTT
SETD8	TRCN0000148268	GTTTCCTGAAACTGGGTTAAT
SETD8	TRCN0000130036	GAATCGCAAACTTACGGATTT
SETDB1	TRCN0000147130	CAGTGACTAATTGTGAGTCTT
SETDB1	TRCN0000179094	CGTGACTTCATAGAGGAGTAT
SETDB2	TRCN0000159172	GCTGAAATTAAAGCCATGCAA
SETDB2	TRCN0000160242	CCTGTTTGTGAAATTAGCTTA
SETMAR	TRCN0000146300	CAAGTGTTCAAGACGCATAAA
SETMAR	TRCN0000179441	GAAAGGCTAGATCATGGGAAA
SMYD1	TRCN0000130695	CGCACATCTTCGGAGTGATTA
SMYD1	TRCN0000130477	GCAATCATGAGGCAGTGAAAT
SMYD2	TRCN0000276083	GCTGTGAAGGAGTTTGAATCA

SMYD2	TRCN0000130403	GCTGTGAAGGAGTTTGAATCA
SMYD2	TRCN0000130774	GCTCTGTGTTTGAGGACAGTA
SMYD3	TRCN0000123292	AGCCTGATTGAAGATTTGATT
SMYD3	TRCN0000123293	CAGCCTGATTGAAGATTTGAT
SMYD4	TRCN0000134109	CCAGAAGATGAAATCCTGTTT
SMYD4	TRCN0000134652	GCTTATGCGTAGATCCTTTAA
SMYD5	TRCN0000155095	GCTATGGGAATTACAACCCAT
SMYD5	TRCN0000156306	CTGTGACACTCTGGAGTTGAA
SUV39H1	TRCN0000158337	CGTTGGGATTCATGGCCTATT
SUV39H1	TRCN0000157251	GCAGGTGTACAACGTCTTCAT
SUV39H2	TRCN0000006938	GCACAGATTGCTTCTTTCAAA
SUV39H2	TRCN0000011057	GCCCACCTTCAGACTTCTATT
SUV420H1	TRCN0000359162	CATCTAAGCTAACTCATATAA
SUV420H1	TRCN0000359230	TTGGTTCTTGATCCCTATTTA
SUV420H2	TRCN0000437411	TGACCCTTGACTCCAGCATAG
SUV420H2	TRCN0000446372	GTGTCCACTCGTGCTTGGAAA
SUV420H2	TRCN0000145137	GAATGACTTCAGCATCATGTA
SUV420H2	TRCN0000143270	GTGTGACCTCATCTTTCTCAT
L3MBTL1	TRCN0000353634	ATCGGATAAAGATCCACTTTG